Journal of Visualized Experiments

Scattering and Absorption of Light in Planetary Regoliths

--Manuscript Draft--

Article Type:	Invited Methods Article - JoVE Produced Video
Manuscript Number:	JoVE59607R2
Full Title:	Scattering and Absorption of Light in Planetary Regoliths
Keywords:	light scattering; light absorption; multiple scattering; radiative transfer; small particles; dense random media; asteroid; comet; planetary regolith; scattering experiment; acoustic levitation; ultrasonic sample control
Corresponding Author:	Karri Muinonen, Ph.D. University of Helsinki Helsinki, Uusimaa FINLAND
Corresponding Author's Institution:	University of Helsinki
Corresponding Author E-Mail:	karri.muinonen@helsinki.fi
Order of Authors:	Karri Muinonen, Ph.D.
	Timo Väisänen
	Julia Martikainen
	Johannes Markkanen
	Antti Penttilä
	Maria Gritsevich
	Jouni Peltoniemi
	Jürgen Blum
	Joonas Herranen
	Gorden Videen
	Göran Maconi
	Petteri Helander
	Ari Salmi
	Ivan Kassamakov
	Edward Haeggström
Additional Information:	
Question	**Response**
Please indicate whether this article will be Standard Access or Open Access.	Open Access (US$4,200)
Please indicate the **city, state/province, and country** where this article will be **filmed**. Please do not use abbreviations.	Helsinki, Finland

TITLE:

Scattering and Absorption of Light in Planetary Regoliths

AUTHORS & AFFILIATIONS:

Karri Muinonen[1,2], Timo Väisänen[1], Julia Martikainen[1], Johannes Markkanen[3,1], Antti Penttilä[1], Maria Gritsevich[1,4], Jouni Peltoniemi[2,1], Jürgen Blum[5], Joonas Herranen[1], Gorden Videen[6,7], Göran Maconi[1], Petteri Helander[1], Ari Salmi[1], Ivan Kassamakov[1], and Edward Haeggström[1]

[1]Department of Physics, University of Helsinki, Finland

[2]Finnish Geospatial Research Institute FGI, National Land Survey, Masala, Finland

[3]Max Planck Institute for Solar System Research, Göttingen, Germany

[4]Institute of Physics and Technology, Ural Federal University, Ekaterinburg, Russia

[5]Institut für Geophysik und Extraterrestrische Physik, Technische Universität Braunschweig, Braunschweig, Germany

[6]Space Science Institute, Boulder, Colorado, USA.

[7]Army Research Laboratory, Adelphi, Maryland, USA.

Email addresses:

Karri Muinonen: karri.muinonen@helsinki.fi

Timo Väisänen: timo.h.vaisanen@helsinki.fi

Julia Martikainen: julia.martikainen@helsinki.fi

Johannes Markkanen: markkanen@mps.mpg.de

Antti Penttilä: antti.i.penttila@helsinki.fi

Maria Gritsevich: maria.gritsevich@helsinki.fi

Jouni Peltoniemi: jouni.peltoniemi@nls.fi

Jürgen Blum: j.blum@tu-bs.de

Joonas Herranen: joonas.herranen@helsinki.fi

Gorden Videen: gorden.videen@gmail.com

Göran Maconi: goran.maconi@helsinki.fi

Petteri Helander: petteri.helander@helsinki.fi

Ari Salmi: ari.salmi@helsinki.fi

Ivan Kassamakov: ivan.kassamakov@helsinki.fi

Edward Haeggström: edward.haeggström@helsinki.fi

Corresponding author:

Karri Muinonen (karri.muinonen@helsinki.fi)

KEYWORDS:

light scattering, light absorption, multiple scattering, radiative transfer, particles, dense random media, asteroid, comet, planetary regolith, scattering experiment, acoustic levitation, ultrasonic sample control

SHORT ABSTRACT:

Numerical and experimental methods are presented for multiple scattering of light in discrete random media of densely-packed particles. The methods are utilized to interpret the

observations of asteroid (4) Vesta and comet 67P/Churyumov-Gerasimenko.

LONG ABSTRACT:

Theoretical, numerical, and experimental methods are presented for multiple scattering of light in macroscopic discrete random media of densely-packed microscopic particles. The theoretical and numerical methods constitute a framework of Radiative Transfer with Reciprocal Transactions (R^2T^2). The R^2T^2 framework entails Monte Carlo order-of-scattering tracing of interactions in the frequency space, assuming that the fundamental scatterers and absorbers are wavelength-scale volume elements composed of large numbers of randomly distributed particles. The discrete random media are fully packed with the volume elements. For spherical and nonspherical particles, the interactions within the volume elements are computed exactly using the Superposition T-Matrix Method (STMM) and the Volume Integral Equation Method (VIEM), respectively. For both particle types, the interactions between different volume elements are computed exactly using the STMM. As the tracing takes place within the discrete random media, incoherent electromagnetic fields are utilized, that is, the coherent field of the volume elements is removed from the interactions. The experimental methods are based on acoustic levitation of the samples for non-contact, non-destructive scattering measurements. The levitation entails full ultrasonic control of the sample position and orientation, that is, six degrees of freedom. The light source is a laser-driven white-light source with a monochromator and polarizer. The detector is a mini-photomultiplier tube on a rotating wheel, equipped with polarizers. The R^2T^2 is validated using measurements for a mm-scale spherical sample of densely-packed spherical silica particles. After validation, the methods are applied to interpret astronomical observations for asteroid (4) Vesta and comet 67P/Churyumov-Gerasimenko (**Figure 1**) recently visited by the NASA Dawn mission and the ESA Rosetta mission, respectively.

INTRODUCTION:

Asteroids, cometary nuclei, and airless solar system objects at large are covered by planetary regoliths, loose layers of particles of varying size, shape, and composition. For these objects, two ubiquitous astronomical phenomena are observed at small solar phase angles (the Sun–object–observer angle). First, the brightness of the scattered light in the astronomical magnitude scale is observed to increase nonlinearly toward the zero phase angle, commonly called the opposition effect[1,2]. Second, the scattered light is partially linearly polarized parallel to the scattering plane (the Sun-object-observer plane), commonly called negative polarization[3]. The phenomena have been lacking quantitative interpretation since late 19th century for the opposition effect and since early 20th century for the negative polarization. Their proper interpretation is a prerequisite for the quantitative interpretation of the photometric, polarimetric, and spectrometric observations of airless objects, as well as radar scattering from their surfaces.

It has been suggested[4–7] that the coherent backscattering mechanism (CBM) in multiple scattering is at least partly responsible for the astronomical phenomena. In the CBM, partial waves, interacting with the same scatterers in opposite order, always interfere constructively in the exact backscattering direction. This is due to the coinciding optical paths of the reciprocal waves. In other directions, the interference varies from destructive to constructive. Configurational averaging within a discrete random medium of particles results in enhanced

backscattering. As for the linear polarization, the CBM is selective and results in negative polarization in the case of positively polarizing single scatterers, a common characteristic in single scattering (cf. Rayleigh scattering, Fresnel reflection).

Scattering and absorption of electromagnetic waves (light) in a macroscopic random medium of microscopic particles has constituted an open computational problem in planetary astrophysics[8,9]. As illustrated above, this has resulted in the absence of quantitative inverse methods to interpret ground-based and space-based observations of solar system objects. In the present manuscript, novel methods are presented for bridging the gap between the observations and their modeling.

Experimental measurements of scattering by a small-particle sample in a controlled position and orientation (six degrees of freedom) has remained open. Scattering characteristics for single particles have been earlier measured as ensemble averages over the size, shape, and orientation distribution[10] by introducing a particle flow through the measurement volume. Scattering characteristics for single particles in levitation have been carried out using, for example, electrodynamic levitation[11] and optical tweezers[12–14]. In the present manuscript, a novel experimental method based on ultrasonic levitation with full control of the sample position and orientation is offered[15].

The present manuscript summarizes the findings of a project funded for five years in 2013–2018 by the European Research Council (ERC): Scattering and Absorption of ElectroMagnetic waves in ParticuLate media (SAEMPL, ERC Advanced Grant). SAEMPL succeeded in meeting its three main goals: first, novel numerical Monte Carlo methods were derived for multiple scattering by discrete random media of densely-packed particles[16–18]; second, novel experimental instrumentation was developed and constructed for controlled laboratory measurements of validation samples in levitation[15]; third, the numerical and experimental methods were applied to interpret astronomical observations[19,20].

In what follows, protocols for utilizing the experimental scattering pipeline for measurements, the corresponding computational pipeline, as well as the application pipelines are described in detail. The computational pipeline consists of software for asymptotically exact computations in the case of finite systems of particles (Superposition *T*-Matrix Method STMM[21] and Volume Integral Equation Method VIEM[22]) and approximate computations for asymptotically infinite discrete random media of particles using multiple scattering methods (SIRIS[23,24], Radiative Transfer with Coherent Backscattering RT-CB[8,9], and Radiative Transfer with Reciprocal Transactions R^2T^2 [16–18]). The experimental pipeline encompasses the preparation, storage, and utilization of the samples, their levitation in the measurement volume, and performing the actual scattering measurement across the range of scattering angles with varying polarizer configurations. The application pipeline concerns the utilization of the computational and experimental pipelines in order to interpret astronomical observations or experimental measurements.

PROTOCOL:

1. Light scattering measurement

1.1. Setting up the scatterometer for measurement (Figure 2)

1.1.1. Turn on the light source, photo-multiplier tubes (PMTs), and amplifiers. Allow the system to stabilize for 30 min.

1.1.2. Align and center the incident beam with pinholes. Two pinholes are attached at pre-measured points on the rotating breadboard, 180° apart and at the same radius. Center the beam on the first pinhole and adjust its angle such that the light also enters through the second pinhole.

1.2. Setting up the acoustic sample levitator

1.2.1. Calibrate the phased array acoustic levitator by measuring the acoustic pressure for each array element in the intended levitation spot as a function of the driving voltage. Use this calibration to compensate for differences between the array channels. Position the calibration microphone by centering its shadow both in the beam and in a perpendicular beam created with two mirrors.

1.2.2. Calculate the driving parameters for the array that create an asymmetric acoustic trap and supply them to the signal generation electronics. This is accomplished by minimizing the Gor'kov potential[25] and aligning the pressure gradients in the levitation spot.

1.2.3. Before inserting the sample, make a measurement sweep with an empty levitator. This reveals any signals generated by ambient light, reflections from the surroundings, and electrical noise.

1.3. Sample handling, insertion, and measurement

1.3.1. Inject the sample into the levitator with an acoustically transparent mesh spoon.

1.3.2. Inspect the orientation and the stability of the sample before and after the scattering measurement with a video camera carrying high-magnification optics. The strength and asymmetry of the acoustic trap are optimized for maximum sample stability: low acoustic power is associated with increased stability.

1.3.3. If the sample is asymmetric, rotate it around the vertical axis to gain information about its shape. Perform the rotation by slowly changing the alignment of the acoustic trap. Apply additional illumination to improve the image quality.

1.3.4. Close the measurement chamber to block out external light.

1.3.5. Using the computer interface, select the orientation of the sample, as well as the angular

resolution and range of the measurement. The incident and the scattered light are filtered by linear polarizers, which are motorized. The measurement sweep is automated, measuring four points for each angle with polarizer angles (0°, 0°), (0°, 90°), (90°, 90°), and (90°, 0°).

1.3.6. Repeat each sweep three times to eliminate outliers. For asymmetric samples, repeat the measurement at different sample orientations.

1.3.7. Recover the sample after the measurement by switching off the acoustic field and letting the sample fall on acoustically transparent fabric. Execute another measurement sweep with empty levitator to detect any possible drifting on the ambient light conditions.

1.3.8. Save and analyze the data. Calculate Mueller matrix elements for each angle through linear combination of intensities at different polarizations[15].

2. Modeling the mm-sized densely-packed spherical media consisting of spherical particles

2.1. Connect into the CSC – IT Center for Science Ltd.'s cluster Taito via SSH access.

2.2. Move into the working directory by executing **cd $WRKDIR**.

2.3. Download sources files with git (git clone git@bitbucket.org:planetarysystemresearch/protocol2.git protocol2).

2.4. Move into the newly created directory **cd protocol2**.

2.5. Download and compile required programs by running **bash compile.sh**, which are preconfigured for Taito.

2.6. Set parameters for a single scatterer, volume element, and the studied sample to match the studied sample by modifying the file **PARAMS** with text editor nano.

2.7. Run pipeline by executing a command **bash run.sh**.

2.8. Write the full Mueller matrix of the sample into **/tmp/final.out**.

3. Interpreting the reflectance spectra for asteroid (4) Vesta

3.1. Deriving the complex refractive indices for howardite.

3.1.1. Download SIRIS4 (git clone git@bitbucket.org:planetarysystemresearch/siris4.2.git).

3.1.2. Compile by executing **make** in the src-folder. Rename the executable **siris42** to **siris4**.

3.1.3. In **mainGo.f90**, change line 395 to **r0=0.05*rmax*sqrt(ran2)**. Compile by executing **make**.

3.1.4. Download the needed MATLAB scripts by executing "git clone git@bitbucket.org:planetarysystemresearch/protocol4a.git".

3.1.5. Copy the executable files created in steps 3.1.2. and 3.1.3. to JoVEOptimize-folder.

3.1.6. Go to folder JoVEOptimize.

3.1.7. In **input1.in** file, set the radius to 30 µm for the howardite particle size, and fix the real part of the refractive index to 1.8. In **input2.in** file, set the radius to 15,000 µm.

3.1.8. Estimate the upper and lower boundaries for the imaginary part of the refractive indices and save them into two separate files. The code utilizes the bisectioning method and uses these values as the starting point.

3.1.9. In **optimizek.m** file, set the file names of the upper and lower boundaries of the $\mathrm{Im}(n)$ and the file name of the measured reflectance spectrum of the howardite powder. Set the wavelength range to 0.4–2.5 µm with 0.05-µm steps.

3.1.10. Run **optimizek.m** in MATLAB to obtain the complex refractive indices for howardite (see **Figure 3**). First, the code computes scattering properties for 30-µm sized (radius) howardite particles, and then uses these particles as diffuse scatterers inside a 15,000-µm sized (radius) volume. These steps are repeated for each wavelength until the computed reflectance matches with the measured reflectance.

3.2. Modelling the reflectance spectrum of Vesta.

3.2.1. Computing the scattering properties of howardite particles by utilizing SIRIS4

3.2.1.1. Move **siris4** executable created in step 3.1.2. into the same folder with the input-file and pmatrix-file. Copy the **input_1.in** and **pmatrix_1.in** from the test-folder.

3.2.1.2. In **input_1.in**, set the number of rays to 2,000,000, the number of sample particles to 1000, the standard deviation of radius to 0.17, and the power-law index of the correlation function to 3. Set the real part of the refractive index to 1.8 and use the $\mathrm{Im}(n)$ values derived in 3.1.

3.2.1.3. Run SIRIS4 by executing **./siris4 input_1.in pmatrix_1.in pmatrix_1.in** for each wavelength (0.4–2.5 µm) using a size (diameter) range of 10 to 200 µm with a sampling step of 10 µm.

3.2.2. Average the obtained scattering matrices, single-scattering albedos, and mean-free paths over a power-law size distribution with index 3.2[19,24].

3.2.2.1. Save each computed scattering phase matrix ***P*** (p-matrix) from step 3.2.1.3. into a **pmatrix_x.in** file (where x describes the wavelength number and ranges from 1 to 43 for each particles size) that contains the scattering angles, P_{11}, P_{12}, P_{22}, P_{33}, P_{34}, and P_{44} elements for one wavelength and particle size.

3.2.2.2. Move the pmatrix-files into folders so that each folder represents one particle size and contains the computed p-matrices for all the wavelengths. Name the folders fold1, fold2, …, foldN, where N is the number of particle sizes.

3.2.2.3. Write the scattering and extinction efficiencies q_{sca} and q_{ext}, as well as the equal-projected-area-sphere radius values r_{hit} from the outputQ-files into one file, Qscas.dat.

3.2.2.4. Go to folder JoVEAverage that was downloaded in step 3.1.4.

3.2.2.5. Move the folders and Qscas.dat into the same folder with **AvgPowerLaw.m**.

3.2.2.6. Run **AvgPowerLaw.m** in MATLAB. The code computes averaged scattering matrices, single-scattering albedos, and mean free-path lengths over a power-law size distribution with index 3.2.

3.2.3. Computing the final spectrum of Vesta by utilizing SIRIS4

3.2.3.1. Use diffuse scatterers inside a Vesta-sized volume with refractive index n = 1.0. In the input-file, use the averaged single-scattering albedos and mean free path lengths for internal scatterers.

3.2.4. Run SIRIS4 for each wavelength by executing **./siris4 input.in pmatrix_X.in pmatrix_X.in**, where X is the wavelength. The code reads the averaged scattering matrices computed at step 3.2.2.6 as input for the internal diffuse scatterers. Study the absolute reflectance at a 17.4-degree phase angle.

3.2.5. Obtain Vesta's observed spectra at 17.4-degree phase angle from the NASA Planetary Data System[26].

3.2.6. Scale Vesta's observed spectra to a geometric albedo value of 0.423[27] at 0.55 µm. To get to 17.4 degrees, apply a factor of 0.491 on the scaled spectra[28]. Now both the modelled and the observed spectra are absolute across the whole wavelength range and can be compared.

4. Photometric and polarimetric modelling of (4) Vesta

4.1. Computing scattering properties for volume-elements containing Voronoi-shaped howardite particles

4.1.1. Connect into the CSC – IT Center for Science Ltd.'s cluster Taito via SSH access.

4.1.2. Move into the working directory by executing **cd $WRKDIR**.

4.1.3. Download the source files (git clone git@bitbucket.org:planetarysystemresearch/jvie_t_matrix.git).

4.1.4. Compile by executing **make** in the src-folder.

4.1.5. Generate volume elements that contain Voronoi-shaped howardite particles by using a MATLAB-code **voronoi_element.m**. In voronoi_element.m, set the wavelength to 0.45 µm, N_elems to 128, the size parameter (elem_ka) to 10, power-law index to 3, minimum particle radius to 0.143 µm, maximum particle radius to 0.35 µm, packing density to 30%, and use the derived complex refractive index for howardite.

4.1.6. Run **voronoi_element.m** in MATLAB. The code generates 128 mesh-files for volume-elements with different Voronoi-particle realizations using the power-law size distribution.

4.1.7. Compute T-matrices for the generated volume-elements by using JVIE. In **runarray_JVIE_T.sh**, set array=1-128. The paramaters are k = 13.962634, mesh = *name of the generated mesh in 4.1.6*, T_out = *name of the output T-matrix*, T_matrix = 1, and elem_ka = 10.

4.1.8. Run JVIE by executing **sbatch runarray_JVIE_T.sh**.

4.1.9. Compute averaged scattering properties from the T-matrices computed with the JVIE code. Execute **./multi_T -N_Tin 128** in the same folder where the computed T-matrices are. The code writes the averaged incoherent Mueller matrix into mueller_elem.h5 and the cross-sections and albedo into output.txt.

4.2. RT-CB computations

4.2.1. Download sources files with git (git clone git@bitbucket.org:planetarysystemresearch/protocol4b.git protocol4b).

4.2.2. Move into the downloaded directory **cd protocol4b**.

4.2.3. Download and compile required programs by running **bash compile.sh**.

4.2.4. Copy the averaged input matrix from step 3.2.2.6 to the current working directory.

4.2.5. Copy the averaged input matrix from step 4.1.9 to the current working directory.

4.2.6. Set parameters by modifying the file **PARAMS** with text editor nano.

4.2.7. Run the pipeline by executing **bash run.sh**.

4.2.8. Write the full Mueller matrix into **tmp/rtcb.out**.

5. Interpreting the observations for Comet 67P/Churyumov-Gerasimenko.

5.1. Computing incoherent volume elements with the fast superposition T-matrix method (FaSTMM) for the organic and silicate grains

5.1.1. Execute **./incoherent_input –lambda 0.649 -m_r 2.0 -m_i 0.2 -density 0.3 -lowB 0.075 -upB 0.125 -npower 3 -S_out pmatrix_org.dat**.

5.1.2. Execute **./incoherent_input –lambda 0.649 -m_r 1.6 -m_i 0.0001 -density 0.0375 -lowB 0.6 -upB 1.3 -npower 3 -S_out pmatrix_sil.dat**.

5.2. Computing the average incoherent Mueller matrix (pmatrix.in), albedo (albedo), mean free path (mfp), and coherent effective refractive index (m_eff)

5.2.1. Run matlab. Type commands:

```
Sorg=load('pmatrix_org.dat');
Ssil=load('pmatrix_sil.dat');
S = (Sorg+Ssil)/2; save('pmatrix.in','S','-ascii');
Csca = (Csca_sil + Csca_org)/2;
Cext = (Cext_sil + Cext_org)/2;
albedo = Csca/Cext;
mfp = Vol/Cext;
```

where Csca_org and Cext_org are the incoherent scattering and extinction cross sections from the step 5.1.2, and Csca_sil and Cext_sil are the incoherent scattering and extinction cross sections from the step 5.1.3.

5.2.2. Run **./m_eff(Csca, r)** in the command line to obtain m_eff where r is the radius of the volume element.

5.3. Computing scattering properties for the coma particles.

5.3.1. Set the values from the step 5.2.1 and 5.2.2 (i.e., albedo, mfp, m_eff in the **input.in** file).

5.3.2. Set power-law index for the correlation length to 3.5 in the **input.in** file.

5.3.3. Run SIRIS4 solver (**./siris4 input.in pmatrix.in**) for particle sizes from 5 μm to 100 μm using a step of 5.

5.3.4. Output the coma phase functions from the SIRIS4 solver.

5.4. Computing scattering properties of the nucleus

5.4.1. Averaging the results from step 5.3.4 over the power-law size distribution of index -3

5.4.1.1. Start Matlab. Run averaging routine **powerlaw_ave.m**. The routine outputs are **pmatrix2.in**, albedo and the mean free path.

5.4.1.2. Set the results (albedo, mean free path) from step 5.4.1.1 in the **input.in** file.

5.4.1.3. Set the size to 10^9, and the correlation length to 2.5. Run SIRIS4 (**./siris4 input.in pmatrix2.in**)

5.4.2. Obtain the nucleus phase function.

REPRESENTATIVE RESULTS:

For our experiment, an aggregate nominally consisting of densely-packed ⌀=0.5 µm spherical SiO_2 particles was selected[29,30] and polished further, to approximate a spherical shape, after which it was characterized by weighing and measuring its dimensions (**Figure 4**). The nearly spherical aggregate had a diameter of 1.16 mm and a volume density of 0.47. Light scattering was measured according to step 1. The beam was filtered to 488±5 nm, with a Gaussian spectrum. The measurement was averaged from three sweeps and the empty levitator signal was subtracted from the result.

From the intensities of the four different polarization configurations, we calculated the phase function, the degree of linear polarization for unpolarized incident light $-M_{12}/M_{11}$, and the depolarization M_{22}/M_{11}, as a function of the phase angle (**Figures 5–7**). One known systematic error source of our measurement is the extinction ratio of the linear polarizers, which is 300:1. For this sample, it is, however, adequate so that the leaked polarized light is below the detection threshold.

The numerical modeling consists of multiple software interlinked by scripts which handle the information flow according to the parameters given by the user. The scripts and software are preconfigured to work on the CSC – IT Center for Science Ltd.'s Taito cluster, and the user needs to modify the scripts and Makefiles themselves to get the modeling tool to work on other platforms. The tool starts by running the STMM solver[20], which computes volume element characteristics as described by Väisänen et al.[18]. After that, the scattering and absorption characteristics of the volume element are used as input for two different software. A Mie-scattering solver is used to find the effective refractive index by matching the coherent scattering cross section of the volume element to a Mie sphere of equal size[20]. Then the aggregate is modeled by running the SIRIS4 software with the volume element as a diffuse scatterer and with the effective refractive index on the surface of the aggregate. The coherent backscattering component is added separately because there is no software that can treat effective refractive medium and coherent backscattering simultaneously. Currently, the RT-CB is incapable of accounting for the effective refractive medium, whereas the SIRIS4 is incapable of accounting for coherent backscattering. The coherent backscattering is, however, added to the SIRIS4[23,24] results

approximately by running the volume-element scattering characteristics through the scattering phase matrix decomposition software PMDEC which derives pure Mueller and Jones matrices required for the RT-CB[9]. The coherent backscattering component is then extracted by subtracting the radiative transfer component from the results of the RT-CB. Then, the extracted coherent backscattering component is added to the results obtained from the SIRIS4.

We simulated numerically the properties of the mm-sized (radius 580 μm) SiO_2 aggregate by following step 2. We used two kinds of volume elements, one consisting of nominal equisized particles (0.25 μm) and the other consisting of normally distributed (mean 0.25 μm, standard deviation 0.1 μm) particles truncated to the range of 0.1–0.2525 μm. Introducing the latter distribution of particles is based on the fact that essentially all SiO_2 samples with a given nominal particle size also have a significant alien distribution of smaller particles[31]. In total, 128 volume elements of size $kR_0=10$ were drawn from 128 periodic boxes containing about 10,000 particles packed to the volume density v=47 % each. From the specifications of the material, we have n=1.463+i0 at the wavelength of 0.488 μm, which is the wavelength used in the measurements.

With SIRIS4, the scattering properties of 100,000 aggregates, with radius of 580 μm, standard deviation of 5.8 μm, and with the power-law index of the correlation function 2, were solved and averaged. These results are plotted (see **Figures 5–7**) with the experimental measurements, and an additional simulation without the effective medium. Both choices for the particle distribution produce a match to the measured phase function (see **Figure 5**), although they result in different polarization characteristics as is seen in **Figure 6**. These differences can be used to identify the underlying distribution of the particles in the sample. The best choice is to use the truncated normal distribution instead of the equisized particles (see **Figure 6**). If only normalized phase functions are used, the underlying distributions are indistinguishable (compare **Figures 5–7**). In **Figure 7** for the depolarization, the numerical results have features similar to the measured curve, but the functions are shifted by 10° to the backscattering direction. The effective refractive index positively corrects the results as is seen from the simulations obtained with and without the effective medium (see **Figures 5–7**). The differences in the polarization (**Figure 6**) indicate that the sample has presumably a more complex structure (e.g., a separate mantle and core) than our homogenous model. It is, however, beyond the existing microscopic methods for sample characterization to retrieve the true structure of the aggregate. The coherent backscattering was added separately to the results. The measurements lack visible intensity spike observed at the backscattering angles, but the degree of linear polarization is more negative between 0–30° which cannot be produced without coherent backscattering (compare “distribution” with “no cb”, see **Figures 5–7**).

For solar system applications, we compared the observed Vesta spectra and the modelled spectrum obtained by following protocol 3. The results are shown in **Figure 3** and **Figure 8** and they suggest that howardite particles, with more than 75% of them having a particle size smaller than 25 μm, dominate Vesta’s regolith. Although the overall match is quite satisfactory, the modelled and observed spectra differ slightly: the absorption band centers of the model spectrum are shifted to longer wavelengths, and the spectral minima and maxima tend to be shallow as compared to the observed spectra. The differences in the minima and maxima could

be explained by the fact that mutual shadowing effects among the regolith particles have not been accounted for: the shadowing effects are stronger for low reflectances and weaker for high reflectances and, in the relative sense, would decrease the spectral minima and increase the spectral maxima when accounted for in the modeling. Furthermore, the imaginary part of the complex refractive indices for howardite was derived without taking into account wavelength-scale surface-roughness, and thus the derived values can be too small to explain the spectral minima. When further using these values in our model by utilizing geometric optics, the band depths in the modelled spectrum can become too shallow. These wavelength-scale effects could also play a part at longer wavelengths together with a small contribution from the low-end tail of the thermal emission spectrum. The differences can also be caused by a compositional mismatch of our howardite sample and Vesta minerals and by a different particle size distribution needed for the model. Finally, the reflectance spectra of Vesta were observed at 180–200 K, and our howardite sample was measured in room temperature. Reddy et al.[32] have shown that the absorption band centers shift to longer wavelengths with increasing temperature.

The photometric and polarimetric phase curve observations for asteroid (4) Vesta are from Gehrels[33] and the NASA Planetary Data System's Small Bodies Node (http://pdssbn.astro.umd.edu/sbnhtml), respectively. Their modeling follows step 4 and starts from the particle refractive index and size distribution available from the spectrometric modeling at the wavelength of 0.45 μm. These particles have sizes larger than 5 μm, that is, much larger than the wavelength and are thus in the geometric optics regime, termed large-particle population. For the phase curve modeling, an additional small-particle population of densely-packed subwavelength-scale particles is also incorporated, with due attention paid to avoid conflicts with the spectrometric modeling above.

The complex refractive index has been set to 1.8+i0.000168. The effective particle sizes and single-scattering albedos in the large-particle and small-particle populations equal (9.385 μm, 0.791) and (0.716 μm, 0.8935), respectively. The mean free path lengths in the large-particle and small-particle media are 16.39 μm and 0.56 μm. The large-particle medium has a volume density of 0.4, whereas the small-particle medium has a volume density of 0.3. The fractions of large-particle and small-particle media in the Vesta regolith are assumed to be 99% and 1%, respectively, giving a total single-scattering albedo of 0.815 and a total mean free path length of 12.78 μm. Following step 4, the Vesta geometric albedo at 0.45 μm turns out to be 0.32 in fair agreement with the observations (cf. **Figure 8** when extrapolated to zero phase angle).

Figures 9–11 depict the photometric and polarimetric phase curve modeling for Vesta. For the photometric phase curve (**Figure 10**, left), the model phase curve from RT-CB has been accompanied with a linear dependence on the magnitude scale (slope coefficient -0.0179 mag/°), mimicking the effect of shadowing in a densely-packed, high-albedo regolith. No alteration has been invoked for the degree of polarization (**Figure 10**, right; **Figure 11**). The model successfully explains the observed photometric and polarimetric phase curves and offers a realistic prediction for the maximum polarization near the phase angle of 100° as well as for the characteristics at small phase angles <3°.

It is striking how the minute fraction of the small-particle population is capable of completing the explanation of the phase curves (**Figures 10–11**). There are intriguing modeling aspects involved. First, as shown in **Figure 9** (left), the single-scattering phase functions for the large-particle and small-particle populations are quite similar, whereas the linear polarization elements are significantly different. Second, in the RT-CB computations, both particle populations contribute to the coherent backscattering effects. Third, in order to obtain realistic polarization maxima, there has to be a significant large-particle population in the regolith (in agreement with the spectral modeling). With the current independent mixing of the small-particle and large-particle media, it remains possible to assign a part of the small-particle contribution to the large-particle surfaces. However, in order for coherent backscattering effects to take place and to explain the observations, it is obligatory to incorporate a small-particle population.

The European Space Agency's (ESA) Rosetta mission to the comet 67P/Churyumov-Gerasimenko provided an opportunity to measure the photometric phase function of the coma and the nucleus over a wide phase-angle range within just a few hours[34]. The measured coma phase functions show a strong variation with time and a local position of the spacecraft. The coma phase function has been successfully modelled[20] with a particle model composed of submicrometer-sized organic and silicate grains using the numerical methods (steps 5 and 2) as shown in **Figure 12**. The results suggest that the size distribution of dust varies in the coma due to the comet's activity and the dynamical evolution of the dust. By modelling scattering by a 1-km-sized object whose surface is covered with the dust particles, we have shown that scattering by the nucleus of the comet is dominated with the same type of particles that also dominate the scattering in the coma (**Figure 13**).

FIGURE LEGENDS:

Figure 1: Asteroid (4) Vesta (left) and Comet 67P/Churyumov-Gerasimenko (right) visited by the NASA Dawn mission and by the ESA Rosetta mission, respectively. Image credits: NASA/JPL/MPS/DLR/IDA/Björn Jónsson (left), ESA/Rosetta/NAVCAM (right).

Figure 2: Light scattering measurement instrument. Photo (above) and top view schematic (below) showing: (1) fiber-coupled light source with collimator, (2) focusing lens (optional), (3) bandpass filter for wavelength selection, (4) adjustable aperture for beam shaping, (5) motorized linear polarizer, (6) high-speed camera, (7) high-magnification objective, (8) acoustic levitator for sample trapping, (9) measurement head, comprising an IR filter, motorized shutter, motorized linear polarizer, and a photomultiplier tube (PMT), (10) motorized rotation stage for adjusting measurement head angle, (11) optical flat for Fresnel reflection, (12) neutral density filter, and (13) reference PMT, for monitoring beam intensity. The system is divided into three enclosed compartments to eliminate stray light.

Figure 3: The imaginary part of the refractive index for howardite as a function of wavelength. The imaginary part of the refractive Im(n) obtained for the howardite mineral by following protocol 3.1. The refractive index is utilized in modeling the scattering characteristics of asteroid (4) Vesta.

Figure 4: The measurement sample composed of densely-packed spherical SiO_2 grains. The sample has been carefully polished in order to obtain a nearly spherical shape that allows for both efficient scattering experiments and numerical modeling.

Figure 5: Phase function. The phase functions of the sample aggregate obtained by following the experimental protocols 1 and the numerical modeling step 2. The phase functions are normalized to give unity when integrated from 15.1° to 165.04°.

Figure 6: Degree of linear polarization. As in **Figure 5** for the degree of linear polarization for unpolarized incident light -M_{12}/M_{11} (in %).

Figure 7: Depolarization. As in **Figure 5** for the depolarization M_{22}/M_{11}.

Figure 8: Absolute reflectance spectra. Asteroid (4) Vesta's modelled and observed absolute reflectance spectra at 17.4-degree phase angle**.**

Figure 9: Scattering phase function P_{11} and degree of linear polarization for unpolarized incident light -P_{21}/P_{11} as a function of the scattering angle for volume elements of large grains (red) and small grains (blue) in the regolith of asteroid (4) Vesta. The dotted line indicates a hypothetical isotropic phase function (left) and a zero level of polarization (right).

Figure 10: Observed (blue) and modeled (red) disk-integrated brightness in the magnitude scale as well as the degree of linear polarization for unpolarized incident light as a function of phase angle for asteroid (4) Vesta. The photometric and polarimetric observations are from Gehrels (1967) and the Small Bodies Node of the Planetary Data System (http://pdssbn.astro.umd.edu/sbnhtml), respectively.

Figure 11: Degree of linear polarization. The degree of linear polarization for asteroid (4) Vesta predicted for large phase angles based on the numerical multiple-scattering modeling.

Figure 12: Modelled and measured photometric phase functions in the coma of comet 67P/Churyumov-Gerasimenko. The variations in the measured phase functions in time can be explained by varying dust size distribution in the coma.

Figure 13: Phase functions. Modeled and measured phase functions of the nucleus of comet 67P.

DISCUSSION:

Experimental, theoretical, and computational methods have been presented for light scattering by discrete random media of particles. The experimental methods have been utilized to validate the basic concepts in the theoretical and computational methods. The latter methods have then been successfully applied in the interpretation of astronomical observations of asteroid (4) Vesta and comet 67P/Churyumov-Gerasimenko.

The experimental scatterometer relies on ultrasonically controlled sample levitation that allows for Mueller-matrix measurements for a sample aggregate in a desired orientation. The aggregate can be repeatedly utilized in the measurements, as it is possible to conserve the aggregate after each measurement set. This is the first time that such non-contact, non-destructive scattering measurements are carried out on a sample under full control.

The theoretical and computational methods rely on the so-called incoherent scattering, absorption, and extinction processes in random media. Whereas the exact electromagnetic interactions always occur coherently, within an infinite random medium after configurational averaging, only incoherent interactions remain among volume elements of particles. In the present work, the incoherent interactions among these elements are exactly accounted for by using the Maxwell equations: after subtracting the coherent fields from the fields in free space, it is the incoherent fields within the random medium that remain. The treatment has presently been taken to its complete rigor in that the interactions, as well as the extinction, scattering, and absorption coefficients of the medium, are derived within the framework of incoherent interactions. Furthermore, it has been shown that accounting for the coherent field effects on the interface between the free space and the random medium results in a successful overall treatment for a constrained random medium.

Application of the theoretical and computational methods has been illustrated for experimental measurements of a mm-scale spherical sample aggregate composed of submicron-scale spherical SiO_2 particles. The application shows, unequivocally, that the sample aggregate must be composed of a distribution of particles with varying sizes, instead of being composed of equisized spherical particles. There may be far-reaching consequences of this result for the characterization of random media: it is plausible that the media are significantly more complex than what has been deduced earlier using state-of-the-art characterization methods.

The synoptic interpretation of the spectrum for asteroid (4) Vesta across the visible and near-infrared wavelengths as well as Vesta's photometric and polarimetric phase curves at the wavelength of 0.45 μm shows that it is practical to utilize the numerical methods in constraining the mineral compositions, particle size distributions, as well as regolith volume density from remote astronomical observations. Such retrievals are further enhanced by the simultaneous interpretation of the photometric phase curves for comet 67P/Churyumov-Gerasimenko concerning its coma and nucleus. Finally, realistic modeling of the polarimetric phase curve of 67P has been obtained[20]. There are major future prospects in applying the present methods in the interpretation of observations of solar system objects at large.

There are future prospects for the present combined experimental and theoretical approach. As it is extremely difficult to accurately characterize random media composed of sub-wavelength-scale inhomogeneities, controlled Mueller-matrix measurements can offer a tool for retrieving information on the volume density and particle size distribution in the medium. Quantitative inversion of these physical parameters is facilitated by the novel numerical methods.

ACKNOWLEDGMENTS:

Research supported by the ERC Advanced Grant № 320773. We thank the Laboratory of Chronology of the Finnish Museum of Natural History for the help with sample characterization.

DISCLOSURES:

The authors have nothing to disclose.

REFERENCES:

1. Gehrels T. Photometric studies of asteroids. V. The light-curve and phase function of 20 Massalia. *Astrophysical Journal* **123**, 331–338 (1956).
2. N. P. Barabashev. *Astronomische Nachrichten* **217**, 445 (1922).
3. Lyot, B. Recherches sur la polarisation de la lumiere des planetes et de quelques substances terrestres. *Annales de l'Observatoire de Paris* **8**(1), 1–161 (1956).
4. Shkuratov, Yu. G. Diffractional model of the brightness surge of complex structures. *Kinematika i fizika nebesnyh tel* **4**, 60–66 (1988).
5. Shkuratov, Yu. G. A new mechanism of the negative polarization of light scattered by the surfaces of atmosphereless celestial bodies. *Astronomicheskii vestnik* **23**, 176–180 (1989).
6. Muinonen, K. Electromagnetic scattering by two interacting dipoles. In: *Proceedings of the 1989 URSI Electromagnetic Theory Symposium.* 428–430, Stockholm (1989).
7. Muinonen, K. Light Scattering by Inhomogeneous Media: Backward Enhancement and Reversal of Polarization, *PhD-thesis, University of Helsinki, Finland* (1990).
8. Muinonen, K., Mishchenko, M. I., Dlugach, J. M., Zubko, E., Penttilä, A., and Videen, G. Coherent backscattering numerically verified for a finite volume of spherical particles. *Astrophysical Journal* **760**, 118–128 (2012).
9. Muinonen K. Coherent backscattering of light by complex random media of spherical scatterers: Numerical solution. *Waves in Random Media*. **14**, 365–388 (2004).
10. Muñoz, O., Volten, H., de Haan, J. F., Vassen, W., and Hovenier, J. W. Experimental determination of scattering matrices of olivine and Allende meteorite particles. *Astronomy & Astrophysics* **360**, 777–788 (2000).
11. Sasse, C., Muinonen, K., Piironen, J., and Dröse, G. Albedo measurements on single particles. *Journal of Quantitative Spectroscopy and Radiative Transfer* **55**, 673—681 (1996).
12. Gong, Z., Pan, Y.-L., Videen, G., and Wang, C. Optical trapping and manipulation of single particles in air: Principles, technical details, and applications. *Journal of Quantitative Spectroscopy and Radiative Transfer* **214**, 94–119 (2018).
13. Nieminen, T. A., du Preez-Wilkinson, N., Stilgoe, A. B., Loke, V. L. Y., Bui, A. A. M., and Rubinsztein-Dunlop, H. Optical tweezers: Theory and modelling. *Journal of Quantitative Spectroscopy and Radiative Transfer* **146**, 59–80 (2014).
14. Herranen, J., Markkanen, J., and Muinonen, K. Dynamics of interstellar dust particles in electromagnetic radiation fields: A numerical solution. *Radio Science* **52**(8), 1016–1029 (2017).
15. Maconi, G., *et al.* Non-destructive controlled single-particle light scattering measurement. *Journal of Quantitative Spectroscopy and Radiative Transfer* 204, 159–164 (2018).
16. Muinonen, K., Markkanen, J., Väisänen, T., Peltoniemi, J., and Penttilä, A. Multiple scattering of light in discrete random media using incoherent interactions. *Optics Letters* **43**, 683–686

(2018).
17. Markkanen, J., Väisänen, T., Penttilä, A., and Muinonen, K. Scattering and absorption in dense discrete random media of irregular particles. *Optics Letters* **43**, 2925–2928 (2018).
18. Väisänen, T., Markkanen, J., Penttilä, A., and Muinonen, K. Radiative transfer with reciprocal transactions: Numerical method and its implementation. *Public Library of Science One (PLoS One)* **14***,* e0210155 (2019).
19. Martikainen, J., Penttilä, A., Gritsevich, M., Videen, G., and Muinonen, K. Absolute spectral modelling of asteroid (4) Vesta. *Monthly Notices of the Royal Astronomical Society* **483**, 1952-1956 (2019).
20. Markkanen, J., Agarwal, J., Väisänen, T., Penttilä, A., and Muinonen, K. Interpretation of phase functions of the comet 67P/Churyumov-Gerasimenko measured by the OSIRIS instrument. *Astrophysical Journal Letters* **868**(1), L16. (2018).
21. Markkanen, J., Yuffa, A. J. Fast superposition T-matrix solution for clusters with arbitrarily-shaped constituent particles. *Journal of Quantitative Spectroscopy and Radiative Transfer* **189**, 181–188 (2017).
22. Markkanen, J. and Ylä-Oijala P. Numerical Comparison of Spectral Properties of Volume-Integral-Equation Formulations. *Journal of Quantitative Spectroscopy and Radiative Transfer* **178**, 269-275 (2016).
23. Lindqvist, H., Martikainen, J., Räbinä, J., Penttilä, A., and Muinonen, K. Ray optics for absorbing particles with application to ice crystals at near-infrared wavelengths. *Journal of Quantitative Spectroscopy and Radiative Transfer* **217**, 329–337 (2018).
24. Martikainen, J., Penttilä, A., Gritsevich, M., Lindqvist, H., and Muinonen, K. Spectral modeling of meteorites at UV-vis-NIR wavelengths. *Journal of Quantitative Spectroscopy and Radiative Transfer* **204**, 144–151 (2018).
25. Gor'kov, L. P. On the forces acting on a small particle in an acoustical field in an ideal fluid. *Soviet Physics Doklady* **6** (1962).
26. Reddy, V. Vesta Rotationally Resolved Near-Infrared Spectra V1.0. EAR-A-I0046-3-REDDYVESTA-V1.0. *NASA Planetary Data System* (2011).
27. Tedesco, E. F., Noah, P. V., Noah, M., and Price, S. D. IRAS Minor Planet Survey. IRAS-A-FPA-3-RDR-IMPS-V6.0 *NASA Planetary Data System* (2004).
28. Hicks, M. D., Buratti, B. J., Lawrence, K. J., Hillier, J., Li, J.-Y., Vishnu Reddy, V., Schröder, S., Nathues, A., Hoffmann, M., Le Corre, L., Duffard, R., Zhao, H.-B., Raymond, C., Russell, C., Roatsch, T., Jaumann, R., Rhoades, H., Mayes, D., Barajas, T., Truong. T.-T., Foster, J., McAuley, A. Spectral diversity and photometric behavior of main-belt and near-Earth vestoids and (4) Vesta: A study in preparation for the Dawn encounter. *Icarus* **235**, 60–74 (2014).
29. Weidling, R., Güttler, C., Blum, J. Free collisions in a micro-gravity many-particle experiment. I. Dust aggregate sticking at low velocities. *Icarus* **218**, 688-700 (2012).
30. Blum, J., Beitz, E., Bukhari, M., Gundlach, B., Hagemann, J.-H., Heißelmann, D., Kothe, S., Schräpler, R., von Borstel, I., Weidling, R. Laboratory drop towers for the experimental simulation of dust-aggregate collisions in the early solar system. *Journal of Visualized Experiments (JoVE)* **88**, e51541, doi:10.3791/51541 (2014).
31. Poppe, T., Schräpler, R. Further experiments on collisional tribocharging of cosmic grains. *Astronomy & Astrophysics* **438**, 1-9 (2005).
32. Reddy, V., Sanchez, J. A., Nathues, A., Moskovitz, N. A., Li, J.-Y., Cloutis, E. A., Archer, K.,

Tucker, R. A., Gaffey, M. J., Mann, J. P., Sierks, H., Schade, U. Photometric, spectral phase and temperature effects on Vesta and HED meteorites: Implications for Dawn mission. *Icarus* **217**, 153–168 (2012).

33. Gehrels, T. Minor planets. I. The rotation of Vesta. Photometric studies of asteroids. *Astronomical Journal* **72**, 929–938 (1967).
34. Bertini, I., La Forgia, F., Tubiana, C., Güttler, C., Fulle, M., Moreno, F., Frattin, E., Kovacs, G., Pajola, M., Sierks, H., Barbieri, C., Lamy, P., Rodrigo, R., Koschny, D., Rickman, H., Keller, H. U., Agarwal, J., A'Hearn, M. F., Barucci, M. A., Bertaux, J.-L., Bodewits, D., Cremonese, G., Da Deppo, V., Davidsson, B., Debei, S., De Cecco, M., Drolshagen, E., Ferrari, S., Ferri, F., Fornasier, S., Gicquel, A., Groussin, O., Gutierrez, P. J., Hasselmann, P. H., Hviid, S. F., Ip, W.-H., Jorda, L., Knollenberg, J., Kramm, J. R., Kührt, E., Küppers, M., Lara, L. M., Lazzarin, M., Lin, Z.-Y., Lopez Moreno, J. J., Lucchetti, A., Marzari, F., Massironi, M., Mottola, S., Naletto, G., Oklay, N., Ott, T., Penasa, L., Thomas, N., Vincent, J.-B. The scattering phase function of comet 67P/Churyumov–Gerasimenko coma as seen from the *Rosetta*/OSIRIS instrument. *Monthly Notices of the Royal Astronomical Society* **469**, 404–415 (2017).

Figure

Click here to access/download;Figure;Fig-01.tif

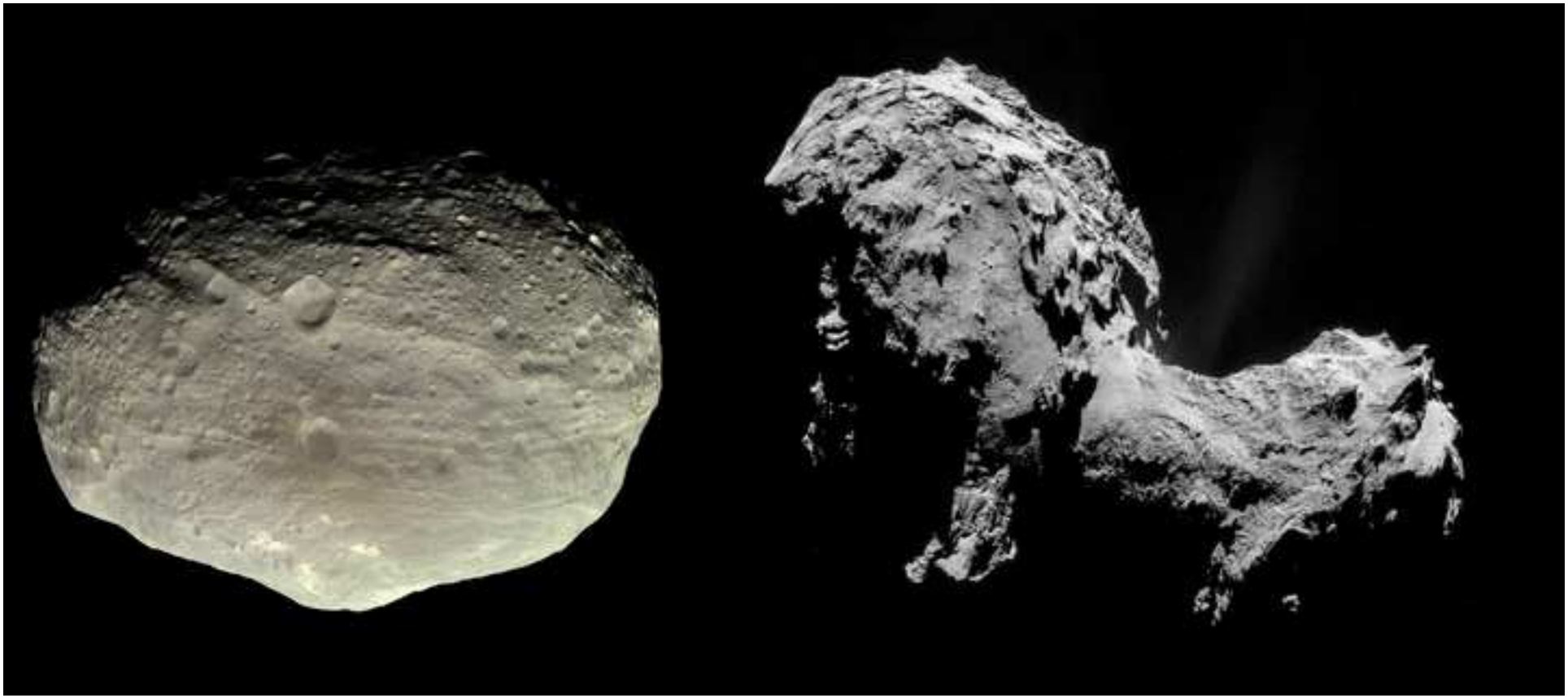

Figure

Click here to access/download;Figure;Fig-02.tif

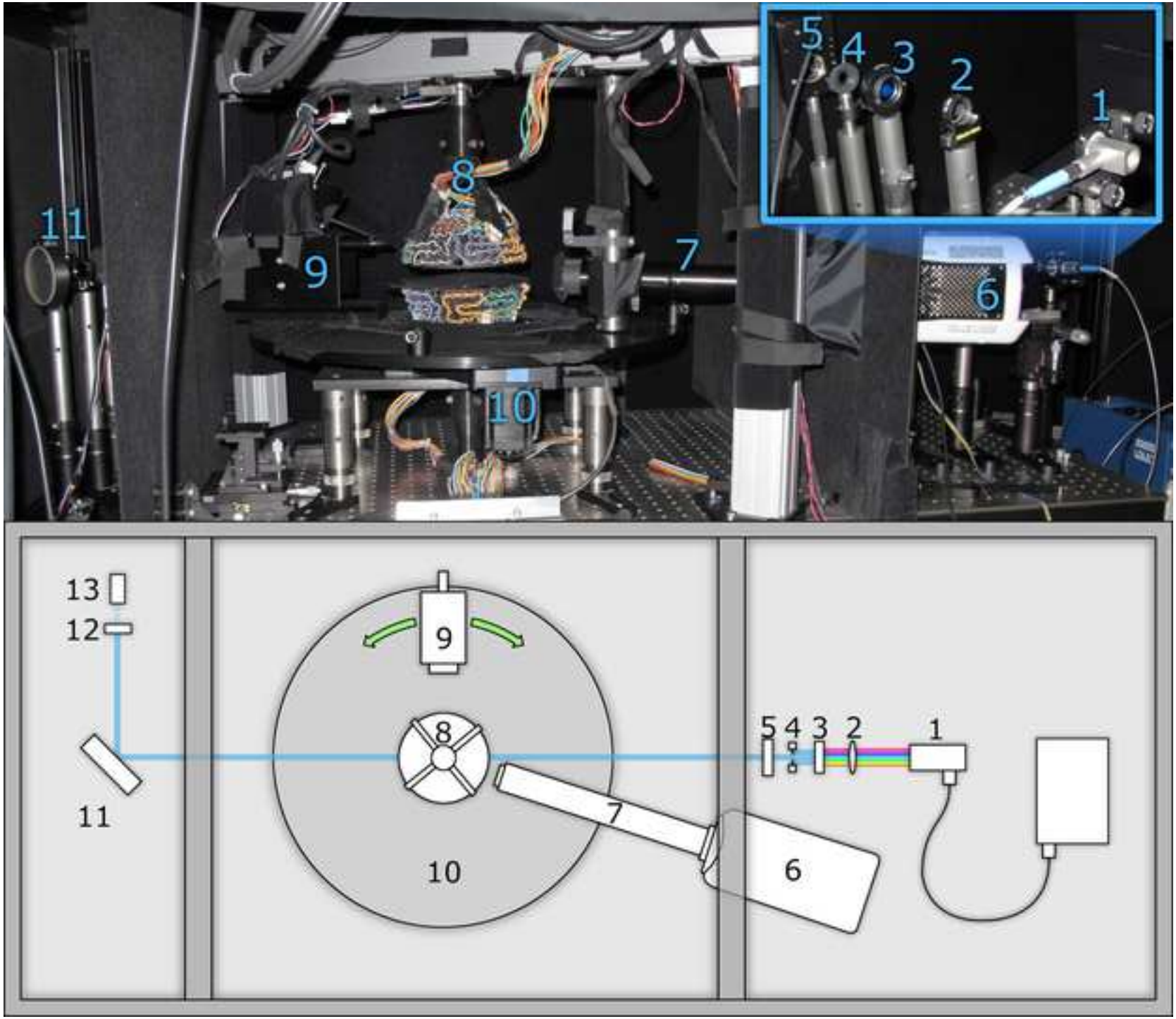

Figure

Click here to access/download;Figure;Fig-3.tif

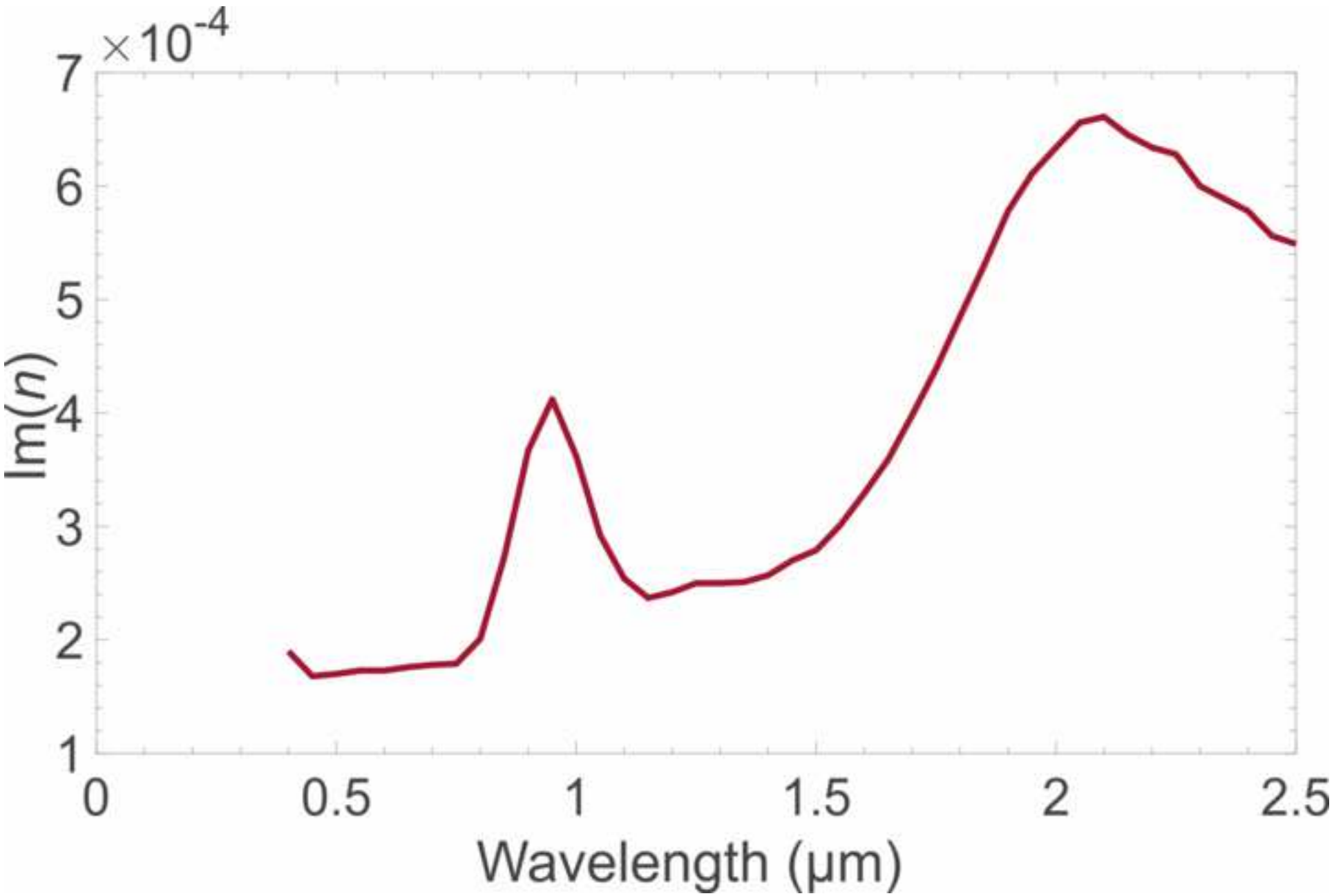

Figure

Click here to access/download;Figure;Fig4.tif

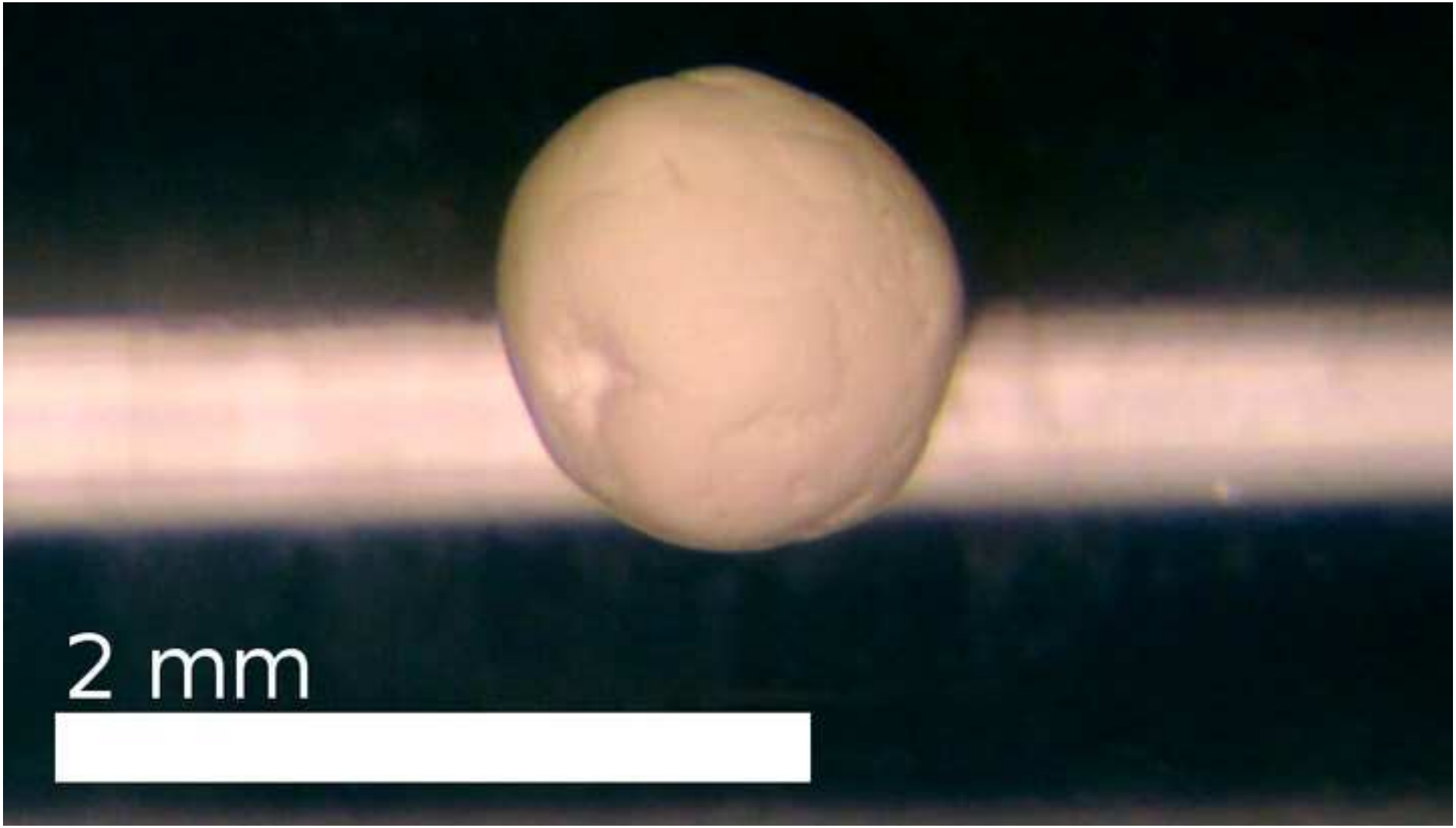

Figure

Click here to access/download;Figure;Fig-5.tif

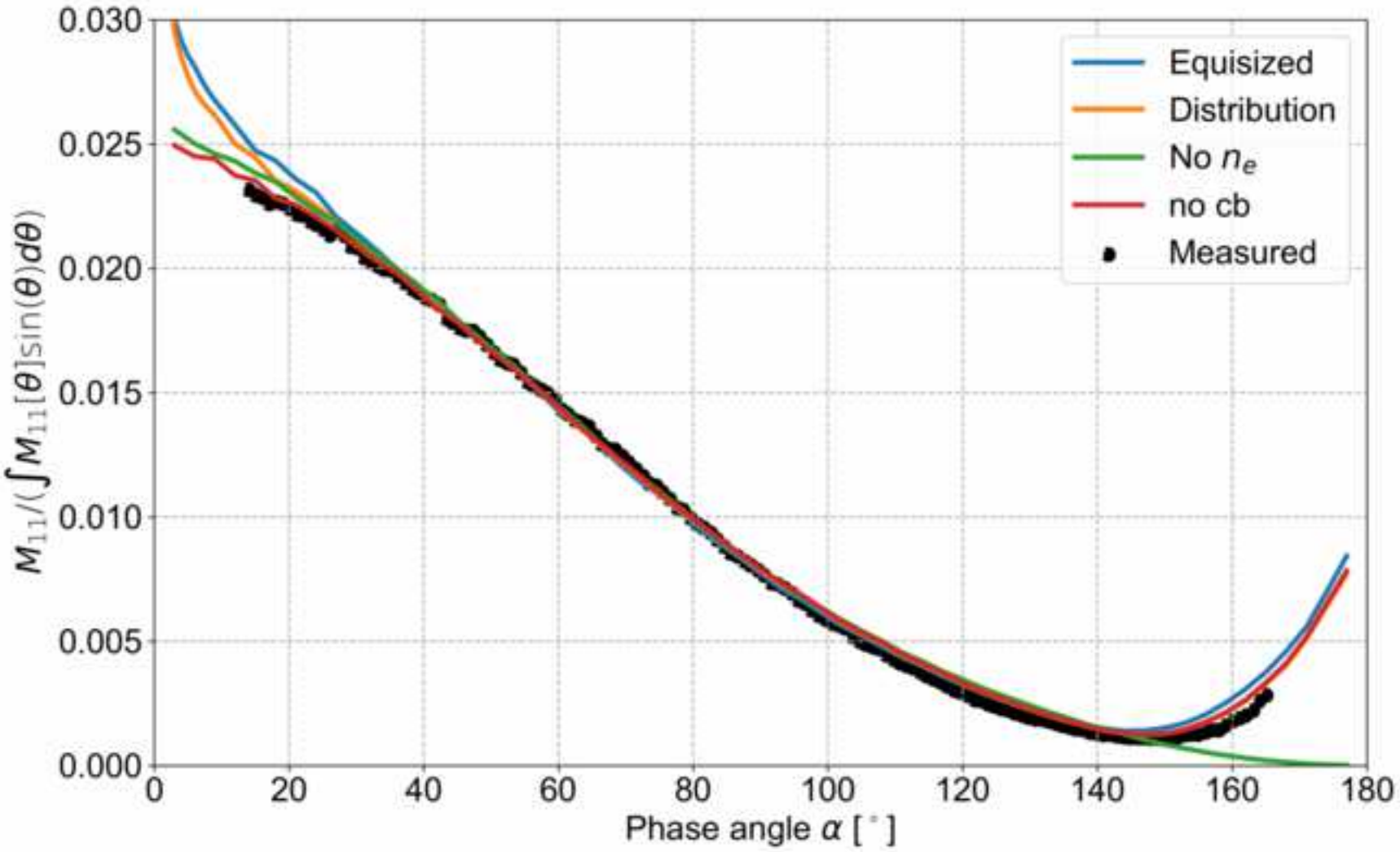

Figure

Click here to access/download;Figure;Fig6.tif

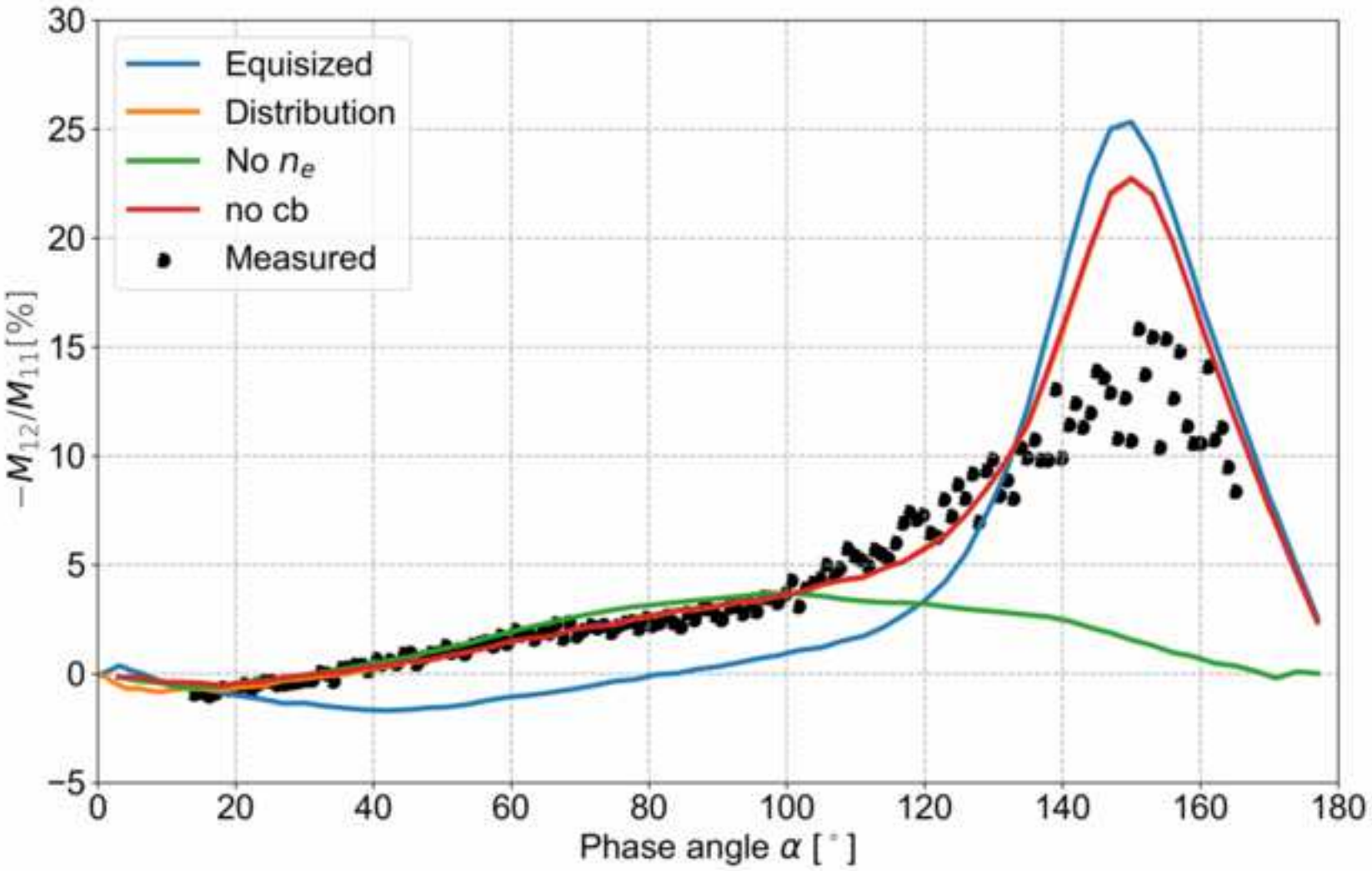

Figure

Click here to access/download;Figure;Fig7.tif

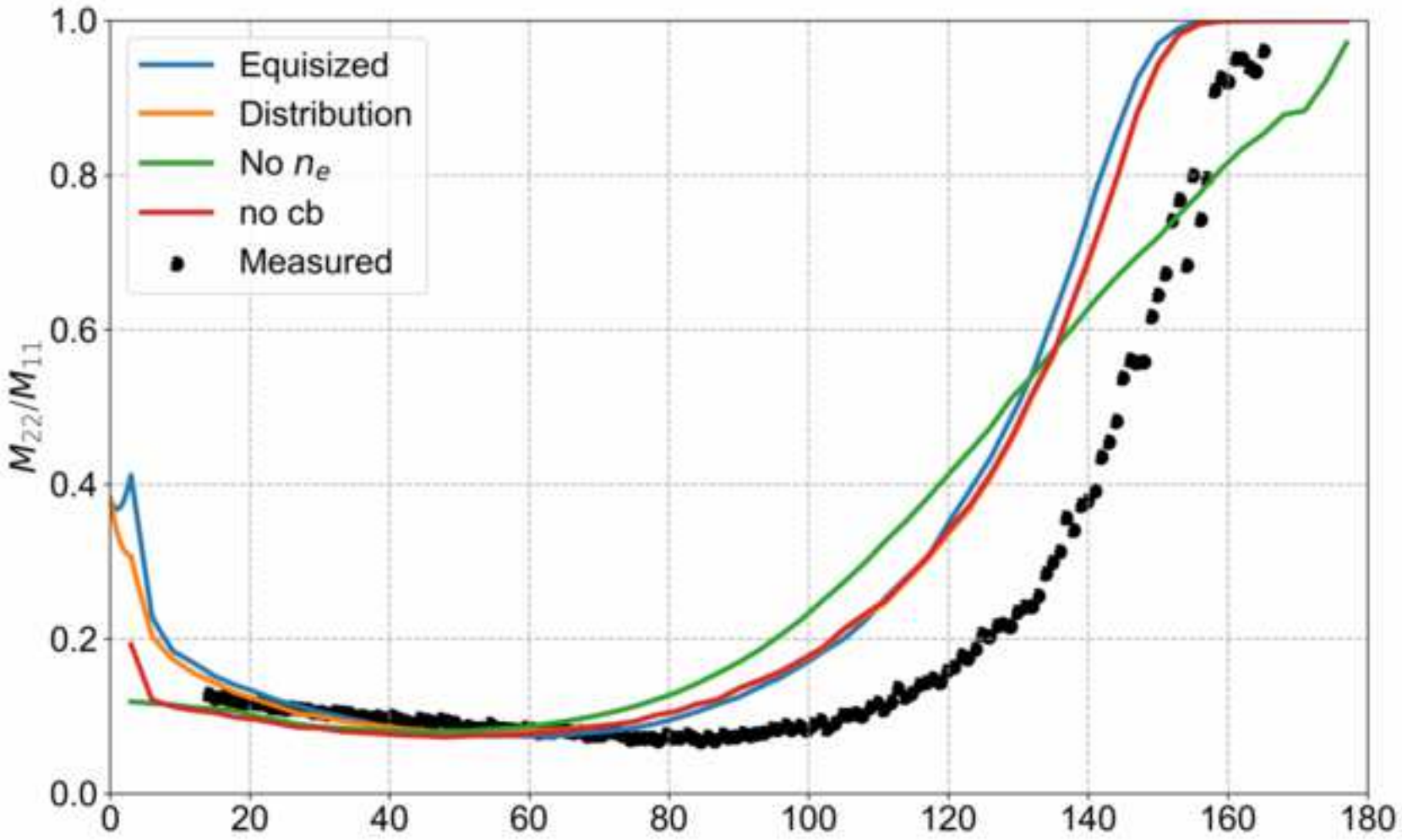

Figure

Click here to access/download;Figure;Fig-08.tif

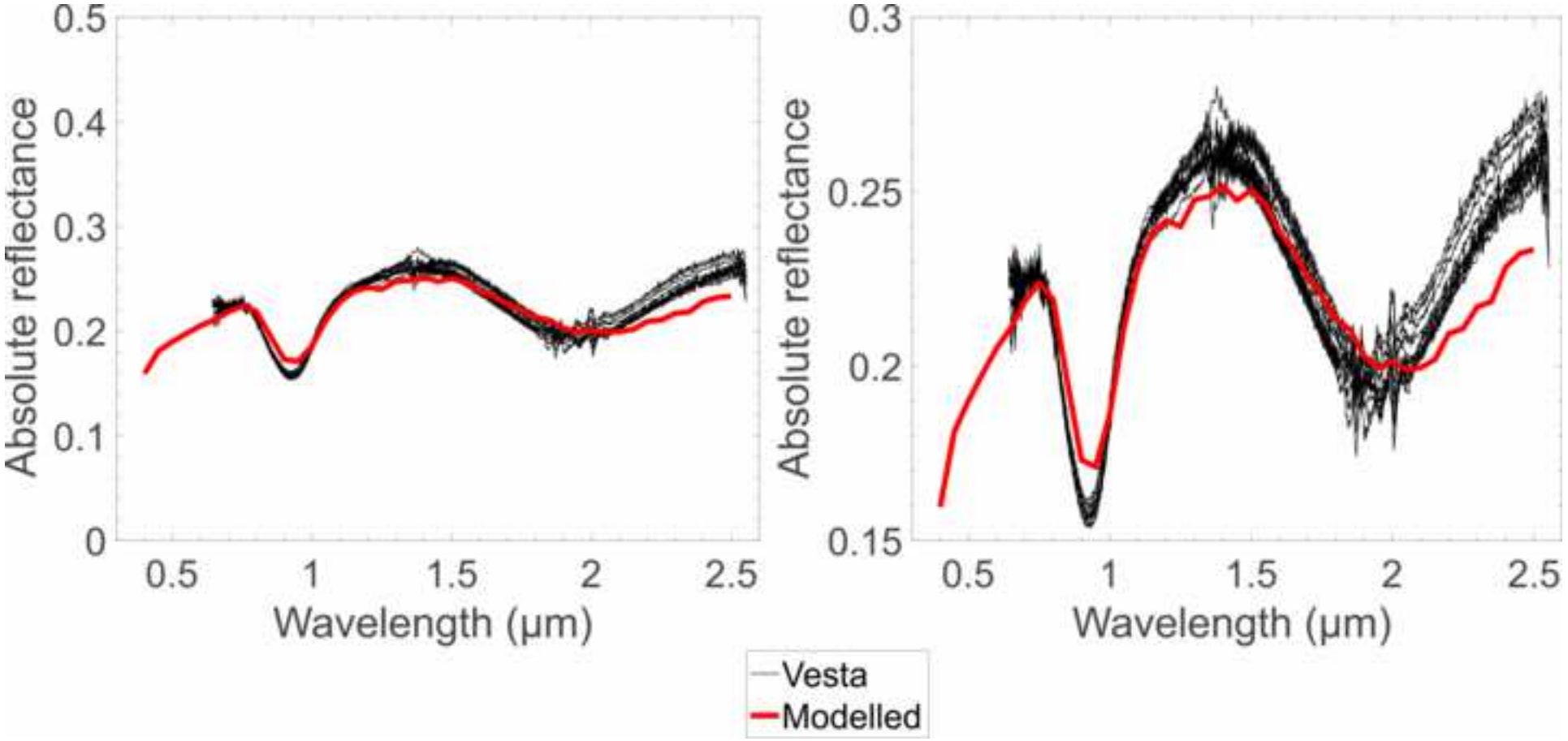

Figure

Click here to access/download;Figure;Fig-09.tif

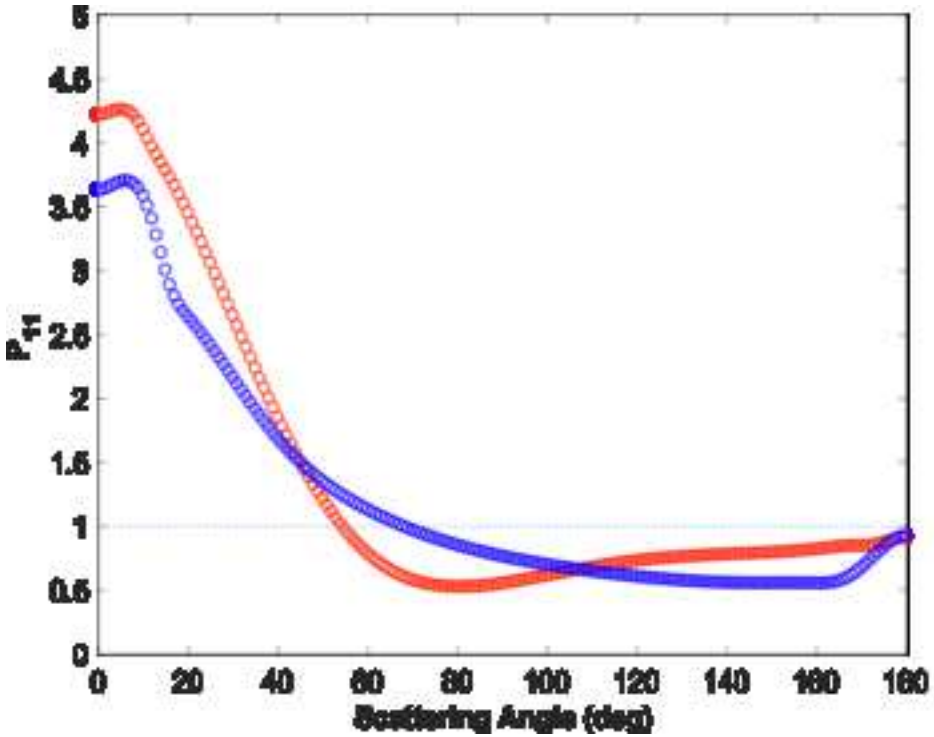

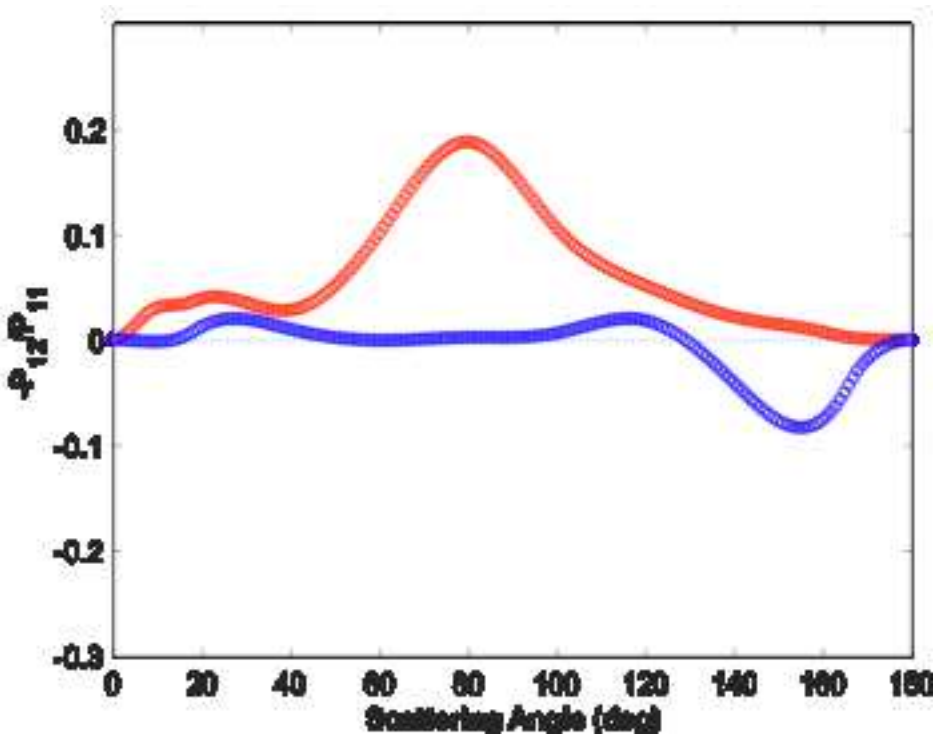

Figure

Click here to access/download;Figure;Fig-10.tif

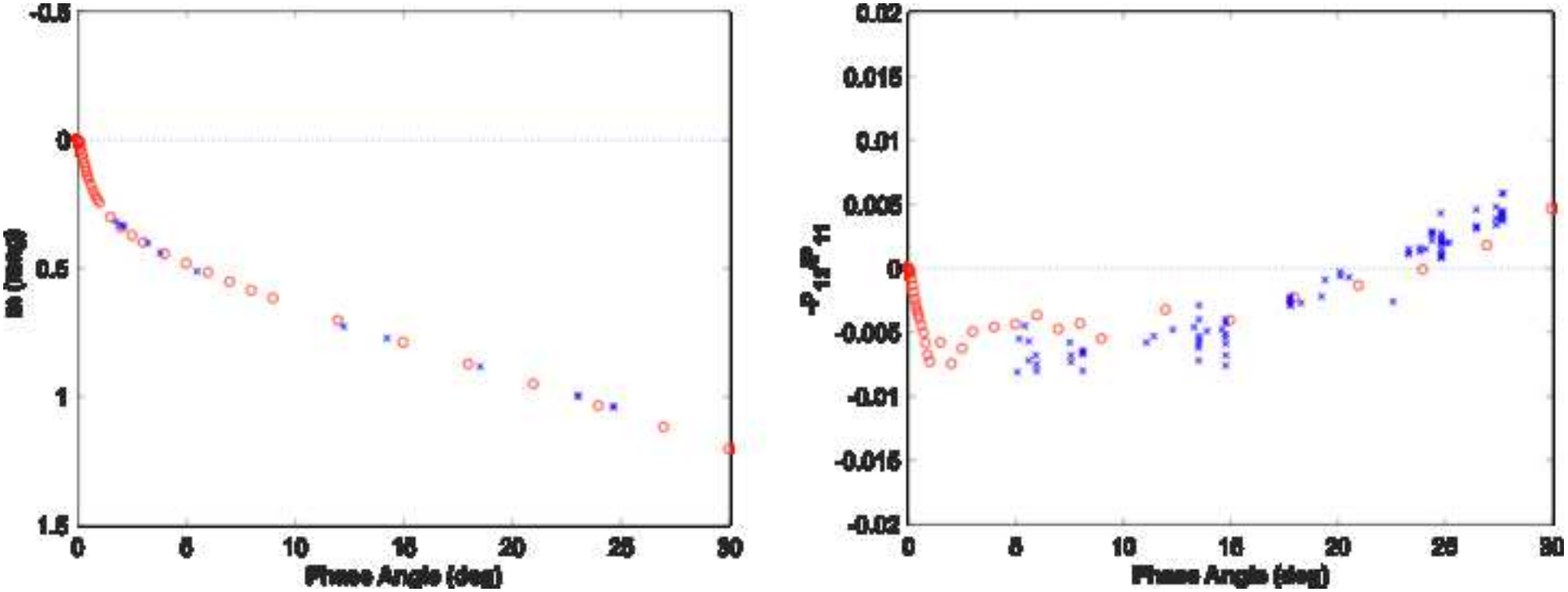

Figure

Click here to access/download;Figure;Fig-11.tif

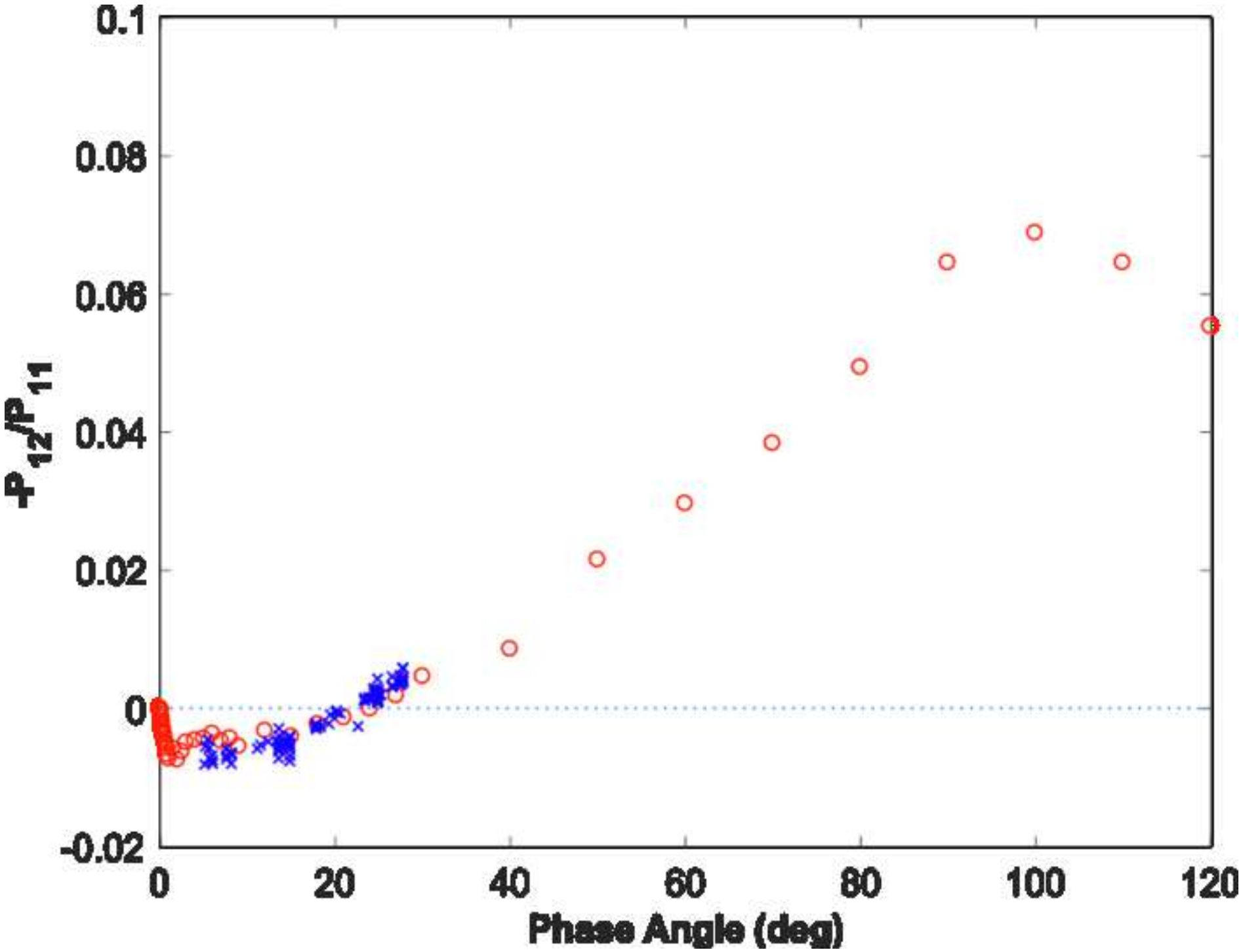

Figure

Click here to access/download;Figure;Fig-12.tif

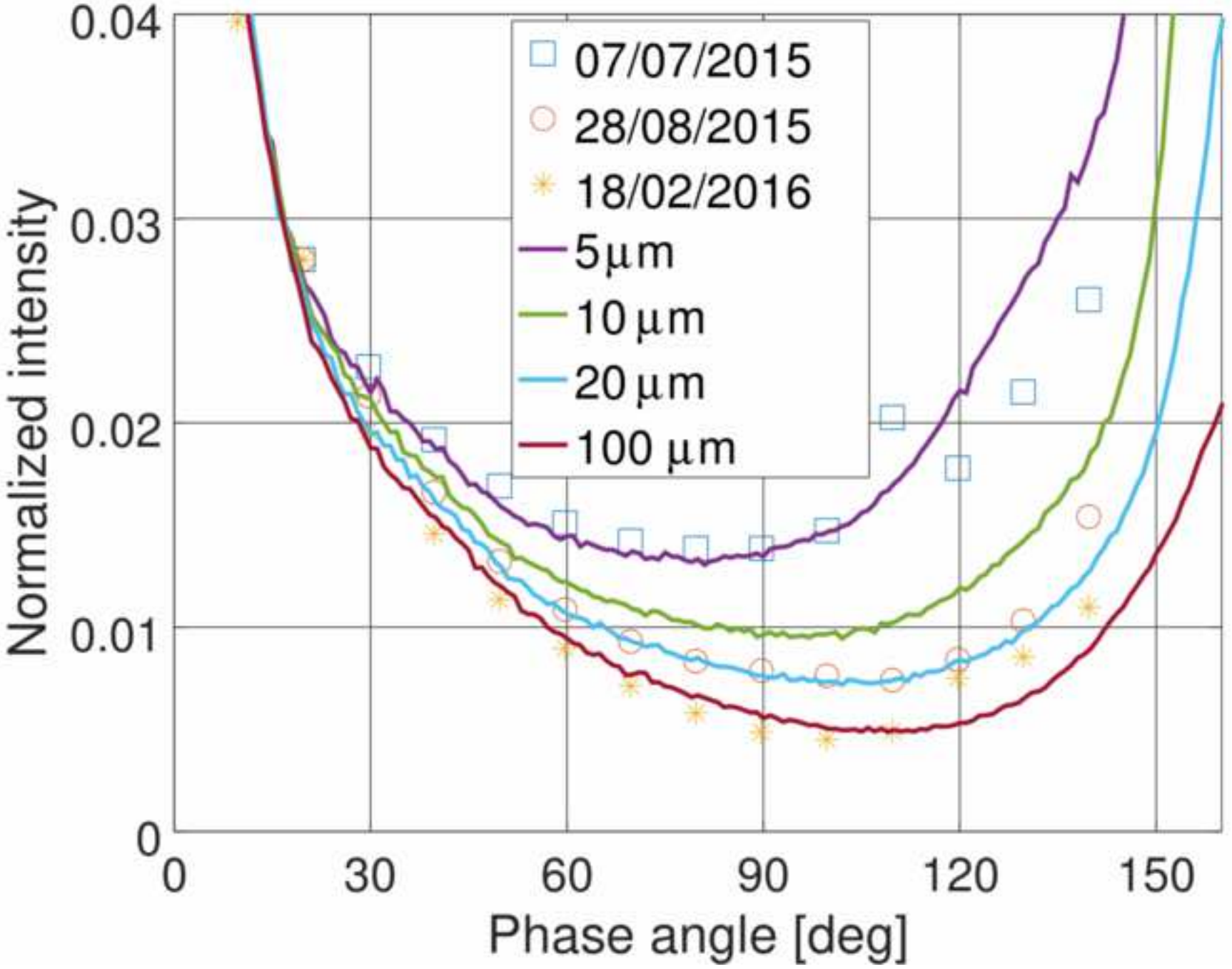

Figure

Click here to access/download;Figure;Fig-13.tif

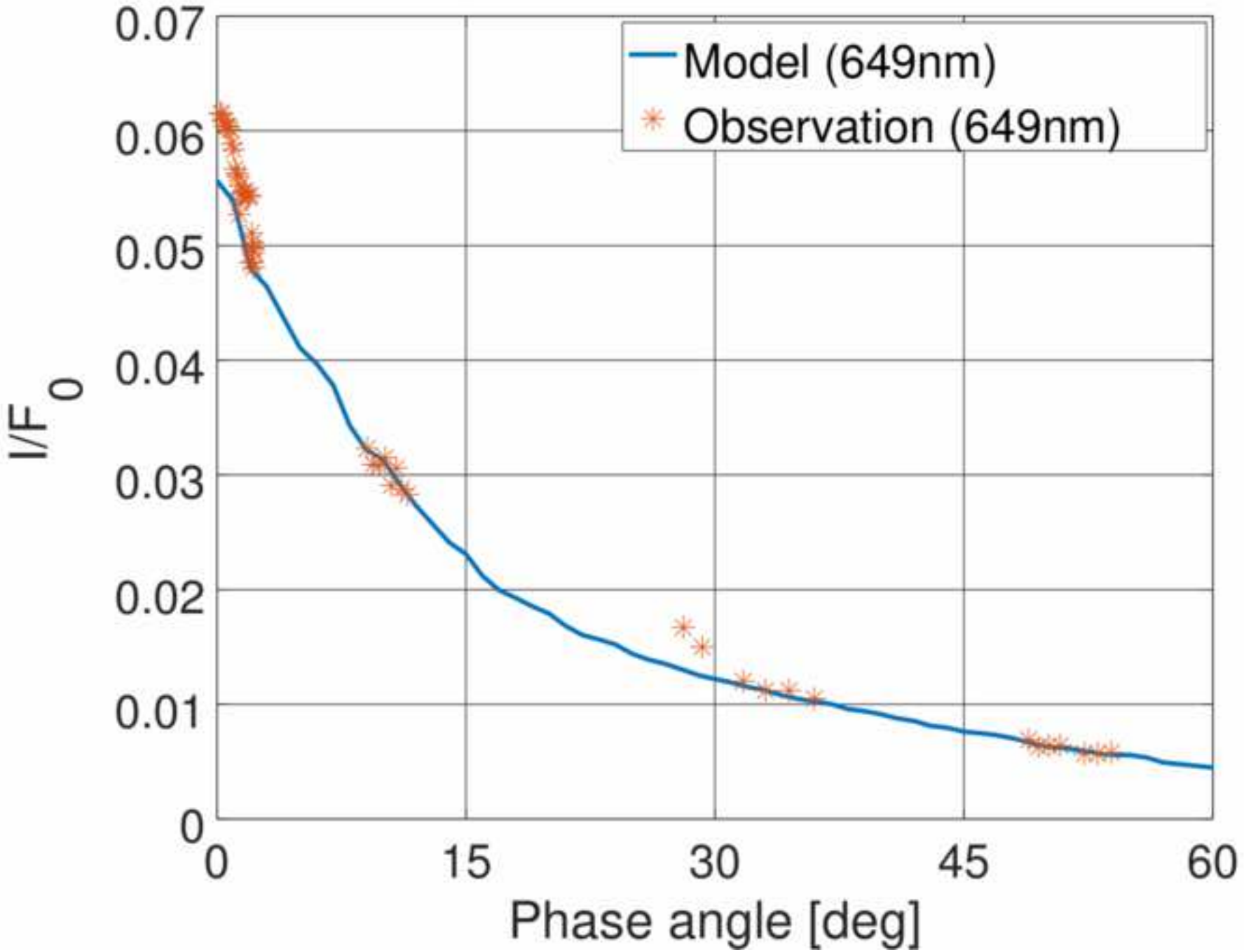

Name of Material/Equipment	Company	Catalog Number	Comments/Description
10GL08	Newport		Calcite polarizer
12X Zoom Body Tube 1-50487AD	Navitar		Microscope objective
43-412-000	Edmund optics		Optical flat
8MPR16-1	Standa		Motorized Polarizer Rotator
8MRB240-152-59D	Standa		Rotation stage
8SMC5-ETHERNET	Standa		Motor controller
Digi-pas DWL3500XY	Digi-pas		Digital 2-axis level
DMT 65-D25-HiDS	Owis		Optics rotation stage
EQ-99 LDLS	Energetiq		Light source
FL488-10	Thorlabs		Laser line filter
IBM 65-D0-35-HiDS	Owis		Motorized iris shutter
LPVISE100-A	Thorlabs		Film polarizer
microPMT H12403-01	Hamamatsu		Photomultiplier tube
NI PXIe-5171R	National Instruments		Digital oscilloscope
NI PXIe-8880	National Instruments		PXIe chassis
Phantom v611	Vision Research		High speed camera
PS 10-32-DC	Owis		Motor controller
RC08FC-P01	Thorlabs		Fiber collimator
SET-NDF-D22-G25	Owis		Neutral density filter
TIA60	Thorlabs		PMT amplifier

jove JOURNAL OF VISUALIZED EXPERIMENTS
1 Alewife Center #200
Cambridge, MA 02140
tel. 617.945.9051
www.jove.com

ARTICLE AND VIDEO LICENSE AGREEMENT

Title of Article: Scattering and absorption of electromagnetic waves in planetary regoliths

Author(s): Karri Muinonen, Timo Väisänen, Julia Markkanen, Johannes Markkanen, Antti Penttilä, Maria Gritsevich, Jouni Peltoniemi, Jürgen Blum, Joonas Herranen, Gorden Videen, Göran Maconi, Petter Helander, Ari Salmi, Ivan Kassamakov, Edward Haeggström

Item 1: The Author elects to have the Materials be made available (as described at http://www.jove.com/publish) via:

☐ Standard Access ☒ Open Access

Item 2: Please select one of the following items:

☒ The Author is **NOT** a United States government employee.

☐ The Author is a United States government employee and the Materials were prepared in the course of his or her duties as a United States government employee.

☐ The Author is a United States government employee but the Materials were NOT prepared in the course of his or her duties as a United States government employee.

ARTICLE AND VIDEO LICENSE AGREEMENT

1. **Defined Terms.** As used in this Article and Video License Agreement, the following terms shall have the following meanings: **"Agreement"** means this Article and Video License Agreement; **"Article"** means the article specified on the last page of this Agreement, including any associated materials such as texts, figures, tables, artwork, abstracts, or summaries contained therein; **"Author"** means the author who is a signatory to this Agreement; **"Collective Work"** means a work, such as a periodical issue, anthology or encyclopedia, in which the Materials in their entirety in unmodified form, along with a number of other contributions, constituting separate and independent works in themselves, are assembled into a collective whole; **"CRC License"** means the Creative Commons Attribution-Non Commercial-No Derivs 3.0 Unported Agreement, the terms and conditions of which can be found at: http://creativecommons.org/licenses/by-nc-nd/3.0/legalcode; **"Derivative Work"** means a work based upon the Materials or upon the Materials and other pre-existing works, such as a translation, musical arrangement, dramatization, fictionalization, motion picture version, sound recording, art reproduction, abridgment, condensation, or any other form in which the Materials may be recast, transformed, or adapted; **"Institution"** means the institution, listed on the last page of this Agreement, by which the Author was employed at the time of the creation of the Materials; **"JoVE"** means MyJove Corporation, a Massachusetts corporation and the publisher of The Journal of Visualized Experiments; **"Materials"** means the Article and / or the Video; **"Parties"** means the Author and JoVE; **"Video"** means any video(s) made by the Author, alone or in conjunction with any other parties, or by JoVE or its affiliates or agents, individually or in collaboration with the Author or any other parties, incorporating all or any portion of the Article, and in which the Author may or may not appear.

2. **Background.** The Author, who is the author of the Article, in order to ensure the dissemination and protection of the Article, desires to have the JoVE publish the Article and create and transmit videos based on the Article. In furtherance of such goals, the Parties desire to memorialize in this Agreement the respective rights of each Party in and to the Article and the Video.

3. **Grant of Rights in Article.** In consideration of JoVE agreeing to publish the Article, the Author hereby grants to JoVE, subject to **Sections 4** and **7** below, the exclusive, royalty-free, perpetual (for the full term of copyright in the Article, including any extensions thereto) license (a) to publish, reproduce, distribute, display and store the Article in all forms, formats and media whether now known or hereafter developed (including without limitation in print, digital and electronic form) throughout the world, (b) to translate the Article into other languages, create adaptations, summaries or extracts of the Article or other Derivative Works (including, without limitation, the Video) or Collective Works based on all or any portion of the Article and exercise all of the rights set forth in (a) above in such translations, adaptations, summaries, extracts, Derivative Works or Collective Works and(c) to license others to do any or all of the above. The foregoing rights may be exercised in all media and formats, whether now known or hereafter devised, and include the right to make such modifications as are technically necessary to exercise the rights in other media and formats. If the "Open Access" box has been checked in **Item 1** above, JoVE and the Author hereby grant to the public all such rights in the Article as provided in, but subject to all limitations and requirements set forth in, the CRC License.

jove JOURNAL OF VISUALIZED EXPERIMENTS
1 Alewife Center #200
Cambridge, MA 02140
tel. 617.945.9051
www.jove.com

ARTICLE AND VIDEO LICENSE AGREEMENT

4. **Retention of Rights in Article.** Notwithstanding the exclusive license granted to JoVE in **Section 3** above, the Author shall, with respect to the Article, retain the non-exclusive right to use all or part of the Article for the non-commercial purpose of giving lectures, presentations or teaching classes, and to post a copy of the Article on the Institution's website or the Author's personal website, in each case provided that a link to the Article on the JoVE website is provided and notice of JoVE's copyright in the Article is included. All non-copyright intellectual property rights in and to the Article, such as patent rights, shall remain with the Author.

5. **Grant of Rights in Video – Standard Access.** This **Section 5** applies if the "Standard Access" box has been checked in **Item 1** above or if no box has been checked in **Item 1** above. In consideration of JoVE agreeing to produce, display or otherwise assist with the Video, the Author hereby acknowledges and agrees that, Subject to **Section 7** below, JoVE is and shall be the sole and exclusive owner of all rights of any nature, including, without limitation, all copyrights, in and to the Video. To the extent that, by law, the Author is deemed, now or at any time in the future, to have any rights of any nature in or to the Video, the Author hereby disclaims all such rights and transfers all such rights to JoVE.

6. **Grant of Rights in Video – Open Access.** This **Section 6** applies only if the "Open Access" box has been checked in **Item 1** above. In consideration of JoVE agreeing to produce, display or otherwise assist with the Video, the Author hereby grants to JoVE, subject to **Section 7** below, the exclusive, royalty-free, perpetual (for the full term of copyright in the Article, including any extensions thereto) license (a) to publish, reproduce, distribute, display and store the Video in all forms, formats and media whether now known or hereafter developed (including without limitation in print, digital and electronic form) throughout the world, (b) to translate the Video into other languages, create adaptations, summaries or extracts of the Video or other Derivative Works or Collective Works based on all or any portion of the Video and exercise all of the rights set forth in (a) above in such translations, adaptations, summaries, extracts, Derivative Works or Collective Works and (c) to license others to do any or all of the above. The foregoing rights may be exercised in all media and formats, whether now known or hereafter devised, and include the right to make such modifications as are technically necessary to exercise the rights in other media and formats. For any Video to which this **Section 6** is applicable, JoVE and the Author hereby grant to the public all such rights in the Video as provided in, but subject to all limitations and requirements set forth in, the CRC License.

7. **Government Employees.** If the Author is a United States government employee and the Article was prepared in the course of his or her duties as a United States government employee, as indicated in **Item 2** above, and any of the licenses or grants granted by the Author hereunder exceed the scope of the 17 U.S.C. 403, then the rights granted hereunder shall be limited to the maximum rights permitted under such statute. In such case, all provisions contained herein that are not in conflict with such statute shall remain in full force and effect, and all provisions contained herein that do so conflict shall be deemed to be amended so as to provide to JoVE the maximum rights permissible within such statute.

8. **Protection of the Work.** The Author(s) authorize JoVE to take steps in the Author(s) name and on their behalf if JoVE believes some third party could be infringing or might infringe the copyright of either the Author's Article and/or Video.

9. **Likeness, Privacy, Personality.** The Author hereby grants JoVE the right to use the Author's name, voice, likeness, picture, photograph, image, biography and performance in any way, commercial or otherwise, in connection with the Materials and the sale, promotion and distribution thereof. The Author hereby waives any and all rights he or she may have, relating to his or her appearance in the Video or otherwise relating to the Materials, under all applicable privacy, likeness, personality or similar laws.

10. **Author Warranties.** The Author represents and warrants that the Article is original, that it has not been published, that the copyright interest is owned by the Author (or, if more than one author is listed at the beginning of this Agreement, by such authors collectively) and has not been assigned, licensed, or otherwise transferred to any other party. The Author represents and warrants that the author(s) listed at the top of this Agreement are the only authors of the Materials. If more than one author is listed at the top of this Agreement and if any such author has not entered into a separate Article and Video License Agreement with JoVE relating to the Materials, the Author represents and warrants that the Author has been authorized by each of the other such authors to execute this Agreement on his or her behalf and to bind him or her with respect to the terms of this Agreement as if each of them had been a party hereto as an Author. The Author warrants that the use, reproduction, distribution, public or private performance or display, and/or modification of all or any portion of the Materials does not and will not violate, infringe and/or misappropriate the patent, trademark, intellectual property or other rights of any third party. The Author represents and warrants that it has and will continue to comply with all government, institutional and other regulations, including, without limitation all institutional, laboratory, hospital, ethical, human and animal treatment, privacy, and all other rules, regulations, laws, procedures or guidelines, applicable to the Materials, and that all research involving human and animal subjects has been approved by the Author's relevant institutional review board.

11. **JoVE Discretion.** If the Author requests the assistance of JoVE in producing the Video in the Author's facility, the Author shall ensure that the presence of JoVE employees, agents or independent contractors is in accordance with the relevant regulations of the Author's institution. If more than one author is listed at the beginning of this Agreement, JoVE may, in its sole

jove JOURNAL OF VISUALIZED EXPERIMENTS
1 Alewife Center #200
Cambridge, MA 02140
tel. 617.945.9051
www.jove.com

ARTICLE AND VIDEO LICENSE AGREEMENT

discretion, elect not take any action with respect to the Article until such time as it has received complete, executed Article and Video License Agreements from each such author. JoVE reserves the right, in its absolute and sole discretion and without giving any reason therefore, to accept or decline any work submitted to JoVE. JoVE and its employees, agents and independent contractors shall have full, unfettered access to the facilities of the Author or of the Author's institution as necessary to make the Video, whether actually published or not. JoVE has sole discretion as to the method of making and publishing the Materials, including, without limitation, to all decisions regarding editing, lighting, filming, timing of publication, if any, length, quality, content and the like.

12. **Indemnification.** The Author agrees to indemnify JoVE and/or its successors and assigns from and against any and all claims, costs, and expenses, including attorney's fees, arising out of any breach of any warranty or other representations contained herein. The Author further agrees to indemnify and hold harmless JoVE from and against any and all claims, costs, and expenses, including attorney's fees, resulting from the breach by the Author of any representation or warranty contained herein or from allegations or instances of violation of intellectual property rights, damage to the Author's or the Author's institution's facilities, fraud, libel, defamation, research, equipment, experiments, property damage, personal injury, violations of institutional, laboratory, hospital, ethical, human and animal treatment, privacy or other rules, regulations, laws, procedures or guidelines, liabilities and other losses or damages related in any way to the submission of work to JoVE, making of videos by JoVE, or publication in JoVE or elsewhere by JoVE. The Author shall be responsible for, and shall hold JoVE harmless from, damages caused by lack of sterilization, lack of cleanliness or by contamination due to the making of a video by JoVE its employees, agents or independent contractors. All sterilization, cleanliness or decontamination procedures shall be solely the responsibility of the Author and shall be undertaken at the Author's expense. All indemnifications provided herein shall include JoVE's attorney's fees and costs related to said losses or damages. Such indemnification and holding harmless shall include such losses or damages incurred by, or in connection with, acts or omissions of JoVE, its employees, agents or independent contractors.

13. **Fees.** To cover the cost incurred for publication, JoVE must receive payment before production and publication of the Materials. Payment is due in 21 days of invoice. Should the Materials not be published due to an editorial or production decision, these funds will be returned to the Author. Withdrawal by the Author of any submitted Materials after final peer review approval will result in a US$1,200 fee to cover pre-production expenses incurred by JoVE. If payment is not received by the completion of filming, production and publication of the Materials will be suspended until payment is received.

14. **Transfer, Governing Law.** This Agreement may be assigned by JoVE and shall inure to the benefits of any of JoVE's successors and assignees. This Agreement shall be governed and construed by the internal laws of the Commonwealth of Massachusetts without giving effect to any conflict of law provision thereunder. This Agreement may be executed in counterparts, each of which shall be deemed an original, but all of which together shall be deemed to me one and the same agreement. A signed copy of this Agreement delivered by facsimile, e-mail or other means of electronic transmission shall be deemed to have the same legal effect as delivery of an original signed copy of this Agreement.

A signed copy of this document must be sent with all new submissions. Only one Agreement is required per submission.

CORRESPONDING AUTHOR

Name:	Karri Muinonen
Department:	Department of Physics
Institution:	University of Helsinki
Title:	Professor
Signature:	Karri Muinonen
Date:	December 23, 2018

Please submit a **signed** and **dated** copy of this license by one of the following three methods:

1. Upload an electronic version on the JoVE submission site
2. Fax the document to +1.866.381.2236
3. Mail the document to JoVE / Attn: JoVE Editorial / 1 Alewife Center #200 / Cambridge, MA 02140

RESPONSE TO THE COMMENTS BY THE EDITOR AND

Manuscript JoVE59607

We have made all the required changes.

>Editorial comments:

>1. Please take this opportunity to thoroughly proofread the manuscript
>to ensure that there are no spelling or grammar issues.

Done.

>2. There is a 2.75 page limit for filmable content. Please highlight
>2.75 pages or less of the Protocol steps (including headings and
>spacing) in yellow that identifies the essen]al steps of the protocol
>for the video, i.e., the steps that should be visualized to tell the
>most cohesive story of the Protocol.

Done.

>3. Step 5.1.1, 5.1.2: Please write each step in complete sentence and
>in the imperative tense.

Done.

>4. 5.3.4: Please write this step in the imperative tense.

Done.

>5. 5.4.2: Please write this step in the imperative tense.

Done.

>6. Figure 3, Figure 7, Figure 11, Figure 13: For each figure, please
>add a short description of the figure in Figure Legend.

Done.

>7. Figure 7: Please use µm instead of microns.

Done.

>8. Figure 8: Please use µm instead of microns.

Done.

>9. Please do not abbreviate journal titles for references.

The journal titles have been spelled out in full length.

Karri Muinonen
on behalf of all authors
Helsinki, March 22, 2019